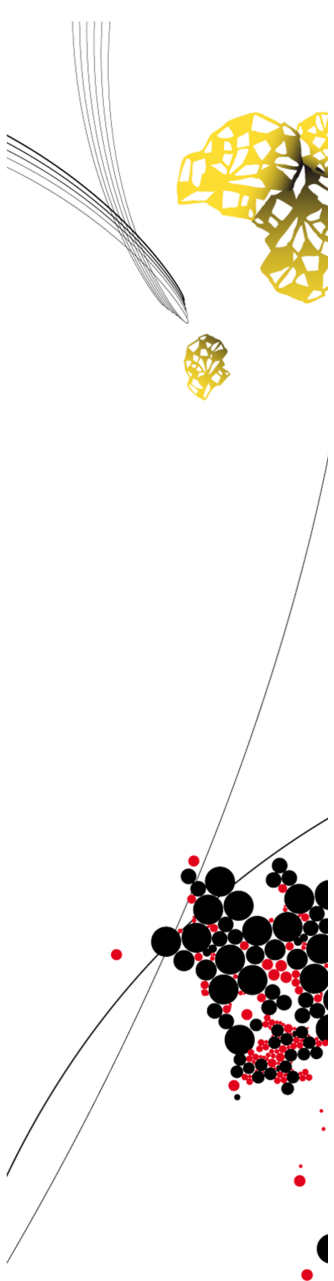


Master Civil Engineering and Management



Initial managed realignment site configuration steer its long-term hydromorphological development

An idealized modelling study

Taj de Vries, s1604961

May 15, 2023

Initial managed realignment site configuration steer its long-term hydromorphological development: an idealized modelling study

Master thesis

University of Twente

Faculty of Engineering Technology

Department of Water Engineering & Management

Author

Taj de Vries

Date:

May 15, 2023

Supervisors

Dr. Ir. B.W. (Bas) Borsje

University of Twente

Ir. R.W.A. (Rutger) Siemes

University of Twente

Dr. Ir. T.M. (Trang) Duong

University of Twente

Abstract

Managed realignment is the landward relocation of a flood defence to re-establish tidal exchange on formerly reclaimed land. The opening of a managed realignment site can help in restoring previously present nature and act as a Nature-based Solution for coastal safety. From a NbS perspective interfering with nature should be kept to a minimum after initial breaching. However, Many recently opened managed realignment sites tend to neglect the effect of initial design on the long-term objective and its effect on the estuary. This study aims to explore and quantify the hydromorphological interplay between the estuary, the inlet and the managed realignment site as a result of dike breaching and reintroducing tidal exchange.

To this end, a idealized 2DH morphological model is set up, resembling a possible location for a managed realignment site behind the Hellegatpolder in the Western Scheldt. The influence of different physical forcings (tidal constituents, sediment concentrations) and initial design (inlet, basin) on the development of the managed realignment site, inlet area and estuary channel are evaluated over a time span of 25 years. The model is able to produce accretion rates over the first two years (4.1 & 3.1cm) comparable to observations from the Perkpolder (3.2 & 2.6), a similar recently opened managed realignment site in the Western Scheldt .

To determine the equilibrium inlet area below mean sea level (MSL) the regime channel method is introduced. The method is a more physically based analytical approach, as opposed to the more conventional equilibrium relationships. The regime channel method is able to correctly predict the equilibrium inlet area based on observations from the Perkpolder. Additionally, the regime channel method is able to determine inlet area over the full time span (25 years) of morphological development based on model results.

After opening, accretion in the managed realignment site is high. Accretion rates over time as the hydroperiod decreases. The accretion pattern in the managed realignment site is twofold. Firstly, cohesive sediment are able to reach the back of the basin promoting landward infilling. Secondly, non-cohesive sediment eroded from the inlet produce 'humps' of sediment that remain locationally stable over 25 years, indicating the importance of initial system configuration on long-term development. Accretion rates are 34% higher in the top half of the basin as a result of flood dominant flow in the estuary channel. The estuary is pushed away from the managed realignment site due to sedimentation at the end of the inlet. The redirection of flow increases erosion downstream and deposition upstream of the inlet.

When the initial inlet area is closer to equilibrium, the initial redistribution of non-cohesive sediment is almost completely depleted. As a result, the site is able to accrete 2.5cm of cohesive sediment more and the impact of the managed realignment site on the estuary diminishes over the full domain. Increasing the site area increases accretion rates and trapping efficiencies. However, it comes at the cost of an increased impact on the estuary morphology and careful consideration should be made about its impact. The initial design of the managed realignment site thus has a significant impact on its long-term development. For future realignment projects the long-term objective should be taken incorporated in the initial design to maximize the potential and minimize its impact the local system.

Contents

1	Introduction	1
1.1	Problem definition	3
1.2	Research aim and questions	3
1.3	Reading guide	4
2	Method	5
2.1	Study area	5
2.2	Hydromorphological model description	6
2.3	Model setup	7
2.3.1	Schematized bathymetry and domain	7
2.3.2	Boundary conditions	9
2.3.3	Morphodynamic settings	9
2.4	Model validation	11
2.5	Inlet evolution	12
2.5.1	Equilibrium relationships	12
2.5.2	Regime channel method	13
2.5.3	Inlet dimensions performance	14
2.6	Data analysis	14
2.7	Model scenarios	14
3	Regime channel method performance	16
3.1	Measured inlet development Perkpolder	16
3.2	RCM for the Perkpolder	18
4	Results	19
4.1	Hydromorphological model performance	19
4.1.1	Hydrodynamic validation	19
4.1.2	Morphological validation	19
4.2	Hydrodynamics	21
4.3	Opening a tidal basin	22
4.3.1	Inlet dynamics	22
4.3.2	Basin dynamics	24
4.3.3	Frontal inlet area	27
4.3.4	Estuary	29
4.3.5	Interplay	30
4.4	Morphodynamic scenario modelling	31
4.4.1	Inlet dynamics	31
4.4.2	Basin dynamics	33
4.4.3	Estuary dynamics	33
5	Discussion	36
5.1	Reflection on the model and method	36
5.1.1	Hydrodynamic boundary conditions	36
5.1.2	Morphological development	36
5.1.3	Model components	37
5.1.4	Conclusion of static model	38
5.2	Model as part of a larger system	38

5.3	Inlet development	39
5.4	Accretion rates and patterns	41
6	Conclusion	43
7	Recommendations	45
7.1	Insight for managed realignment projects	45
7.2	Model improvements	46
7.3	Additional scenarios	46
	References	48
	Appendices	55
A	Model definition and input	55
A.1	Hydromorphological model description	55
A.2	Sand-mud sediment transport	55
A.3	Grid resolution	56
A.4	Model parameters	57
A.5	Neumann boundary conditions	59
B	Regime channel	60
C	Results	60
C.1	Model artifacts	60
C.2	Hydrodynamics	61

1 Introduction

Estuarine regions are at the interface between rivers and seas. The land surrounding estuaries is often densely populated; in fact, 21 of the world's 30 largest cities are located next to estuaries (Ashworth et al., 2015). Their twentieth-century catchment developments, and population and economic growth have had a significant impact on deltas wherein these estuaries lie (Vörösmarty et al., 2009). A rising sea-level, increased peak discharges and land-subsidence pose an increasing risk for millions living along estuaries and coastlines (Syvitski et al., 2009). Sea-level rise (SLR) increases flood risk (Nicholls et al., 2010) and drowning of intertidal habitat area (Balke et al., 2016; Costanza et al., 1997; de Vriend et al., 2011). In addition, estuaries may become sediment starved due to changing sediment supply and discharge regimes (Dunn et al., 2019), and anthropogenic activities such as groundwater extraction induce accelerated land subsidence compounding natural sinking of the land as a result of e.g. sediment compaction (Minderhoud et al., 2017; Syvitski et al., 2009). The combination of geocentric sea-level rise and land elevation change will enhance relative sea-level rise in estuarine regions (Dunn et al., 2019).

The low-lying hinterland of deltas and estuaries are commonly embanked between dykes to protect from flooding. To provide more habitable land, the dyke is often pushed towards the body of water (de Vriend et al., 2011), affecting natural processes occurring in deltas and estuaries (Temmerman et al., 2015). In particular, the loss of intertidal habitat due to dyke construction has cut off the flanking mudflats and salt marshes that would naturally accrete during inundations, which would otherwise balance out background subsidence (Kirwan et al., 2013; Schuerch et al., 2018) and provide storage space and friction for the tidal wave (Friedrichs, 2011), thereby naturally reducing flood risk. Additionally, channel dredging and sea-level rise reduce friction for the tidal wave, which may lead to further tidal amplification in the estuary (Leuven et al., 2018), further increasing potential flood risk.

Obtaining safety against flooding by conventional engineering structures such as dikes and seawalls (Borsje et al., 2011), often referred to as grey engineering, has limits and research has shown that increasing the dimensions of these structures to keep up with increasing flood risk due to impact of climate change is becoming unsustainable (Schuerch et al., 2018; Temmerman et al., 2013). In fact, highly engineered coastal defences are likely to see the strongest risk increase in the long-term (Tessler et al., 2015). The result is a strong need for innovative, sustainable and cost-effective coastal protection solution that deal with the increased flood risk, while minimizing anthropogenic effects on natural ecosystems (Borsje et al., 2011).

Recent research explores the restoration of salt marshes, or managed realignment, Nature-based Solutions (NBS) increasingly recognized for aiding in flood safety and its ecosystem services (Temmerman et al., 2013). These intertidal estuarine wetlands show a positive feedback between accretion and vegetation growth (Fagherazzi et al., 2012; Temmerman et al., 2005), are able to keep up with SLR under certain circumstances (Kirwan et al., 2016) and can reduce wave load on dikes (Vuik et al., 2019), enhancing natural development and help with coastal safety. To this end, (Hu et al., 2021) state that local management measures can still create opportunity for successful restorations, despite climate change and restoration projects are better able to trap sediments (Liu et al., 2021).

However, the global area of intertidal ecosystems like salt marshes is dwindling with 1-2% per year (Duarte et al., 2008). Salt marshes may drown due to sea level rise (Best et al., 2018), while not able to transgress landward (Hopkinson et al., 2018; Kirwan et al., 2016) and are dependant on sufficient sediment availability (Mariotti, 2020; Willemsen et al., 2018). In addition, the seaward salt marsh erosion is affected by the wave climate (Mariotti, 2020; Willemsen et al.,

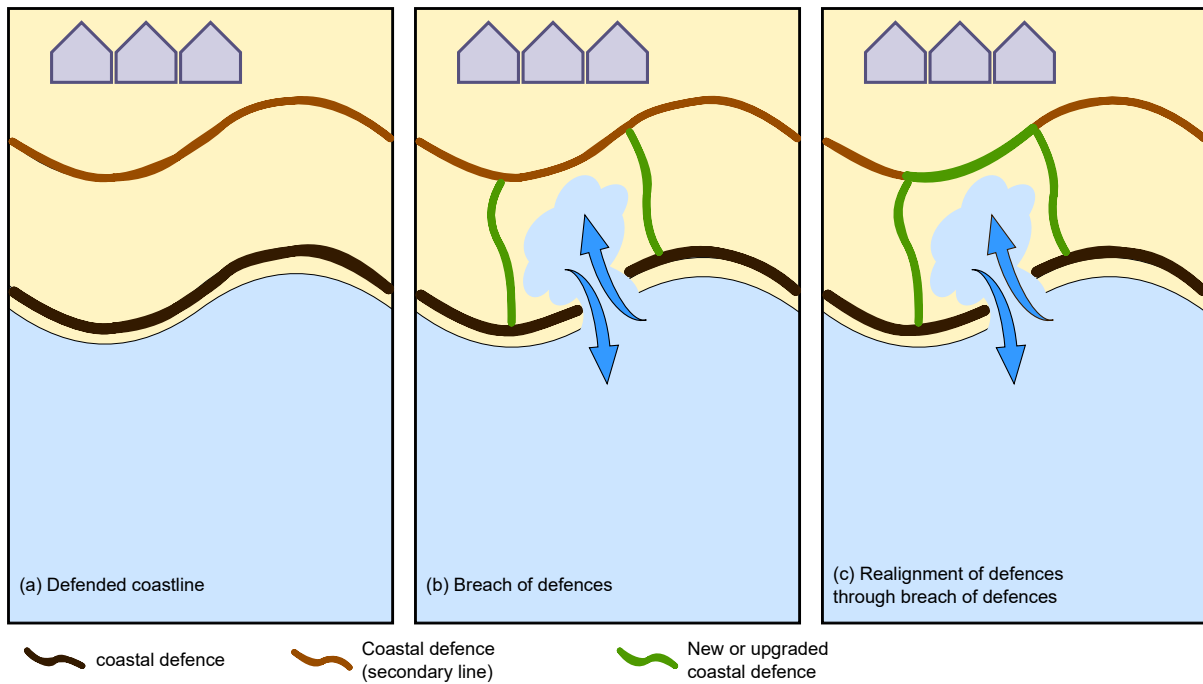


Figure 1.1: Concept of managed realignment by breaching existing seawall and reintroducing tidal exchange (concept after Esteves (2014)). (a) Situation without managed realignment. (b) Seaward dike is breached and cross-shore dikes are built to contain MR site. (c) Seaward dike is breached and new or upgraded dikes are built to contain MR site

2018) and due to sea-level rise these waves are situated higher in the tidal frame, enhancing erosion of the intertidal wetland.

An alternative concept for restoring intertidal wetland is managed realignment (MR). Managed realignment is the landward relocation of flood infrastructure to re-establish tidal exchange on formerly reclaimed land (Bridges et al., 2021). In particular, the focus lies on breaching part of an existing dike, while either relying on already present secondary defences (Figure 1.1b) or upgrading or building new defences (Figure 1.1c). Only partly breaching a dike can have several benefits as opposed to creating more space for intertidal wetland. Firstly, Remnants of the old dike can act as wave breakers (Hofstede, 2019), reducing wave edge erosion and thus increase salt marsh survivability. Secondly, it is easier to restore the function of the old dike when the managed realignment site will be used as a 'transitional polder' (De Mesel et al., 2013; Zhu et al., 2020): a polder that is opened temporarily to elevate the low lying hinterland by intertidal exchange and can later be returned to its original function (e.g. agricultural land). However, knowledge on the interplay between the managed realignment site (MRS), the inlet (or breach) and the estuary and its effect on hydrodynamic and morphological development is limited. Hence, a better understanding on the impact of opening a MRS in an estuarine environment is necessary in order to understand its viability as a Nature-based Solution as opposed to more traditional wetland reclamation projects.

Morphological models can help to explore the development of a MRS after opening. So far, spatially explicit models focus on the driving factors of intertidal wetland development and survival of locations directly adjacent to a body of water (Best et al., 2018; Mariotti, 2020; Willemsen et al., 2018). Modelling studies on MRS with a breach are generally focused on a single case study (Gourgue et al., 2022) or have vastly larger scales (Xu et al., 2022) and tend to neglect the interplay between the MR site, the inlet (or breach) and the body of water it is

connected to, forcing suspended sediment concentrations (SSC) at the inlet based on estuarine measurements, which may lead to errors in the the actual SSC able to reach the MRS. Moreover, these studies neglect the hydrodynamics of the tidal wave propagating through the estuary and its impact on the hydromorphological development and in particular on inlet (or breach) dynamics, whilst breach dimensions can steer the hydromorphological development of the MRS (Friess et al., 2014; Townend et al., 2010). Weisscher et al. (2022) makes use of a morphological model to systematically asses the influence of MRS design choices on a decadal spatial scale and includes estuarine hydrodynamics. However, the coarse grid resolution applied here does not allow for analysis of key features (Williams & Esteves, 2017) such as inlet dynamics and channel formation within the MRS, which may lead to unrealistic sedimentation rates and patterns.

1.1 Problem definition

A number of recently opened managed realignment sites have shown large increases in breach dimensions after opening (de Wilde, 2022; Friess et al., 2014; Pontee et al., 2019), while creating sufficient breach dimensions to encourage flood dominance can positively influence MRS deposition (Townend et al., 2010), indicating a lack of understanding of the effect of design choices. In addition, large sediment releases as a result of high initial breach erosion could have negative indirect impacts on local ecosystems (e.g. smother marine habitats Norkko et al., 2002). The typical temporal scale for geological restoration in a managed realignment scheme can be in the range of 15-60 years (Gerwing et al., 2020; van Belzen et al., 2021; Xu et al., 2022). Breaching an embankment is itself a disturbance, impacting local and regional stable ecosystems that have developed over time (Gerwing et al., 2020) and from a NbS point of view, interfering with nature should be kept to a minimum after the initial breaching. However, the influence of driving physical processes and implementation design on the decadal scale has received little to no attention.

From a managers perspective it would be beneficial to have a more general sense of the effects of design choices under local driving processes to adjust MRS design to its long-term objective. The use of process-based numerical models to determine the decadal hydromorphological development of a MRS under different driving processes and design implementation can increase knowledge and aid coastal managers in accounting for the short and long-term objective of the MRS.

The scope of this work provides an intermediate approach in terms of spatial scale (20km²) to determine the interplay between the estuary, inlet and site hydromorphological development, able to capture the key processes such as inlet development and tidal creek formation (on the scale of typical western Scheldt creeks; Best et al., 2018). To this end, an idealized numerical model will be set up from scratch that will be used to systematically asses the influence of typical wetland development parameters and site design choices. This will provide a more general understanding of the processes that steer the hydromorphological development of MR sites, providing a starting point for designing MR sites to reach their desired objective.

1.2 Research aim and questions

This study aims to explore and quantify the hydromorphological interplay between the estuary, the inlet and the managed realignment site as a result of dike breaching and reintroducing tidal exchange. The response of the hydromorphological development under the influence of different typical wetland parameters and site design choices is assessed systematically.

This leads to the main research question:

To what extent can we steer the hydrodynamic and morphological development of a managed realignment site on the decadal scale?

The main research question is divided into research questions in order to structure the report.

1. What are the driving factors for breach evolution after opening managed realignment site?
2. How does a managed realignment site in an estuarine environment develop on the decadal scale?
3. What is the influence of physical forcings on the hydrodynamic and morphological development of a a managed realignment site?
4. What is the influence of managed realignment site design choices on the hydrodynamic and morphological development of a managed realignment site?

1.3 Reading guide

The research questions are answered based on comparison of the Perkpolder, a recently opened managed realignment site in the Western Scheldt, and the use of an idealized morphological model (using Delft3D-FM, a new generation flexible mesh model). Section 2 describes the methodology of the research. Herein, the model set-up in terms of physical characteristics, schematization of the model domain, and the applied hydro- and morphodynamic forcings is described. In addition, an alternative approach for inlet development is introduced in conjunction with the case study.

Section 3 describes the results of the use of the alternative approach for inlet development for the case study. These results are used as a validation tool for the use of alternative approach for inlet development of the model. The results are explained in Section 4. Firstly, the model is validated and a reference scenario is compared to other managed realignment projects. After, the results of scenarios are explained and their implications for the design of a managed realignment scheme. Section 5 discusses the model results and its implication. Section 6 answers the research question and draws the main conclusion. Section 7 described the recommendation for future research and features a section describing the use of the results for managerial implications.

2 Method

2.1 Study area

The Scheldt Estuary is located at the transition between the North Sea and the Scheldt river in the southern province of Zeeland in the Netherlands (Figure 2.1). The tide penetrates up to the city of Gent in Belgium (~ 180 km from the mouth). The mean tidal range (MTR) varies from 3.65m (meso-tidal) at the Hoofdplaat salt marsh in the west to 4.6m (macro-tidal) at the Zuidgors salt marsh in the east (van der Wal et al., 2008), with tidal flats and shoals interrupted by evasive meandering ebb and straight flood channels (Callaghan et al., 2010). Waves in front of intertidal areas are mostly generated locally and based on wind speed, direction and fetch length (van der Wal et al., 2008). The mean discharge from the Scheldt river is around $100 \text{ m}^3/\text{s}$, on the order of 1/1000 of the tidal prism (de Vriend et al., 2011). The low discharge and relatively weak wind-driven waves make the estuary tide-dominated and well-mixed.

Within this region, the location landward of the Hellegatpolder (Figure 2.1) near the city of Ossenisse is chosen as the location for creating a managed realignment site, also noted as a potential location for creating a MRS by van Belzen et al. (2021) and Weisscher et al. (2022). It is situated approximately 40km from the mouth of the estuary next to the main channel, used as a shipping lane. The Hellegatpolder is an intertidal wetland, where the southern part is partly covered with vegetation and the eastern part fronting the proposed MRS is a bare tidal flat. The difference in vegetation cover is likely caused by predominantly southwesterly winds (van der Wal et al., 2008) that create waves eroding the bare mudflat in the eastern part, while the south part is more sheltered. The hinterland is currently used as agricultural land and bed levels range from 0 tot 1m+NAP. The bed consists of a mixture of light and and medium clay (TNO, 2021), well consolidated due to prior use.

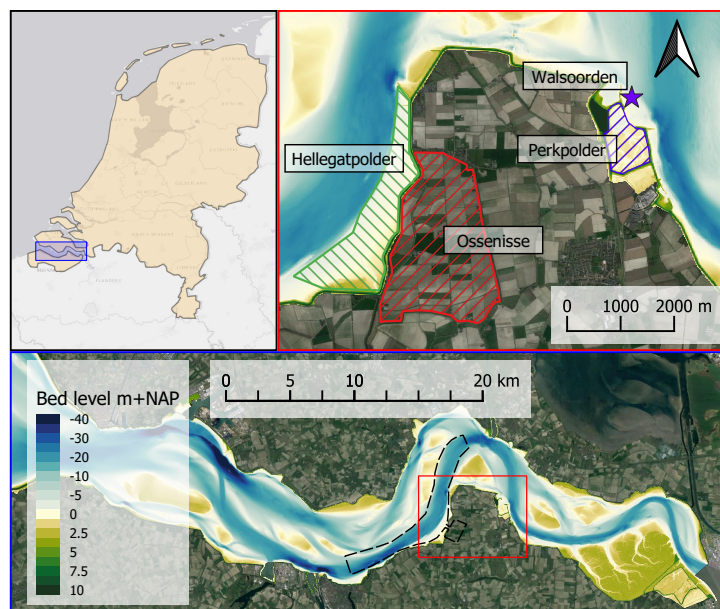


Figure 2.1: Visualization of the study area. **Top left:** Top view of the Netherlands with the location of the Western Scheldt in the blue box. **Bottom:** The Western Scheldt estuary, whereupon model settings are based. The overlay shows the bathymetry from 2021. Dashed black line indicates the extent of the idealized model domain. **Top right:** Location of the Perkpolder, Walsoorden measurement station, Hellegatpolder and possible location for a managed realignment site (based on Weisscher et al., 2022)

2.2 Hydromorphological model description

The Delft3D Flexible Mesh (Delft3D-FM) process-based, numerical model was used in the current study to simulate hydrodynamics, sediment dynamics and morphological processes. This model and its predecessor Delft3D are widely used in coastal, estuarine and riverine systems (Kernkamp et al., 2011; Lesser et al., 2004; Oorschot et al., 2016). A more extensive description of the hydromorphological model and its components can be found in Appendix A.1. The flow module D-Flow FM solves the unsteady shallow-water equations on an unstructured finite volume grid two dimensionally (depth-averaged, 2DH; see Deltares, 2022a).

The D-Morphology module (Deltares, 2022b) controls the transport of sediments and bed-level changes, directly communicating with the flow-module. Erosion and deposition of cohesive sediment are calculated with the Partheniadas-Krone equations (Partheniadas, 1965). The non-cohesive sediment transport is calculated using the equations by van Rijn (2007a, 2007b). The model distinguishes two erosion modes based on a critical mud content ($p_{m,crit}$). Below the critical mud content, the erosion of both sand and mud is governed by the erosion properties of sand. The influence of mud in this mode is governed according to van Rijn (2007a). Above the critical mud content, the erosion of both mud and sand is governed by the erosion properties of mud. The bed is modelled using the stratigraphic module by van Kessel et al. (2011, 2012). This module tracks the spatial and temporal bed composition of layers of a user-defined thickness, with erosion and deposition based on the top transport layer. A detailed explanation about the governing equations for sediment transport, the sand mud interaction and the stratified bed layers is given in section A.2.

Coupling between D-Flow and D-Morphology occurs each numerical time step. Herein, the morphological change is multiplied with an acceleration factor (Roelvink, 2006, MorFac,) of 100 every single time step (Figure 2.2). The computation of a subsequent hydrodynamic time step uses the morphological change multiplied by the acceleration factor. This approach and magnitude of the MorFac has been used in a number of studies (Best et al., 2018; Gourgue et al., 2022; Willemsen et al., 2018). Every 3.65 days of hydrodynamic calculations thus represents the morphological development of a full year, i.e. 91.25 hydrodynamic days represents 25 years of morphological change. A single day of spin-up time is added before morphological change occurs, resulting in a total of 92.25 simulated hydrodynamic days. A full spring-neap cycle of approximately 14.6 days represent the morphological change of 4 years, resulting in 6.25 spring neap cycles. Calculations are performed with Delft3D FM 2023.01 and it is strongly advised to use this or a later version to prevent previously present software instabilities. Running a model scenario takes approximately 4 days (3 cores @2.6Ghz; 16GB RAM).

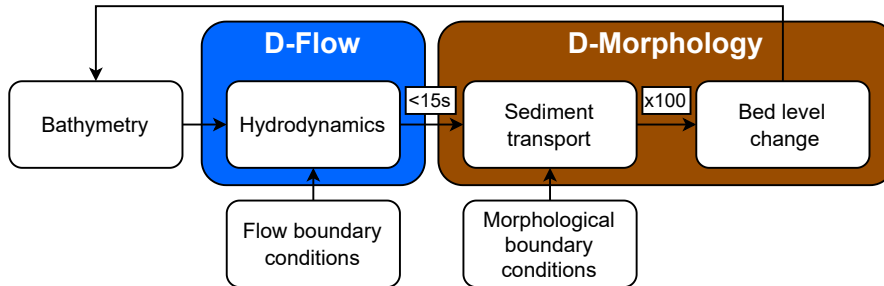


Figure 2.2: Schematic overview of the modules and processes used for hydromorphological simulations. Arrows indicate coupling between modules. Coupling between D-Flow and D-Morphology is always below 15s (Appendix A.4 DtMax) and sediment transport rates are increased by the MorFac = 100

2.3 Model setup

The model domain of the depth-averaged flow model is based on the physical characteristics of the Western Scheldt. It represents an area with an alongshore length of 14km and a cross-shore width of 3.7km (Figure 2.3). The domain consists of a deep estuarine channel, the previously present intertidal wetland, the dike breach creating an inlet and the managed realignment site itself. The channel is in the alongshore direction, such that the tidal flow is propagated through the channel and the MRS is in the cross-shore direction. This represents a typical managed realignment scheme in which space for biogeomorphological development is created.

2.3.1 Schematized bathymetry and domain

A schematized bathymetry was developed from scratch resembling, but not identical to a part of the Western Scheldt at the Hellegatpolder (Figure 2.3). Such simplified schematizations are commonly applied to gain quantitative insights into the real estuarine development (Duong et al., 2017; Siemes et al., in prep.), while limiting model complexity and making observed trends more generic and applicable for other estuaries.

The cross-shore domain starts in the estuary channel at a depth of $-16\text{m}+\text{NAP}$. The bed level increases to $-15\text{m}+\text{NAP}$ over a distance of 1000m to represent the deep estuarine channel fronting the Hellegatpolder. The bed level increases to the local mean sea level ($0.18\text{m}+\text{NAP}$) over a distance of 820m, following a Dean's equilibrium profile (Dean, 1991); fitted using local bathymetry data (RWS, 2023a). After, the bed level increases to $0.5\text{m}+\text{NP}$ up to the toe of the old dike, representing the already present wetland in front of the dike over a distance of 180 meters. Sharp changes in bed level gradients between the estuary channel and the equilibrium profile, and the equilibrium profile and the wetland showed unnatural bed level development. To prevent this numerical instability, bed level gradients were smoothed out around these transitions (following van der Wegen et al., 2017).

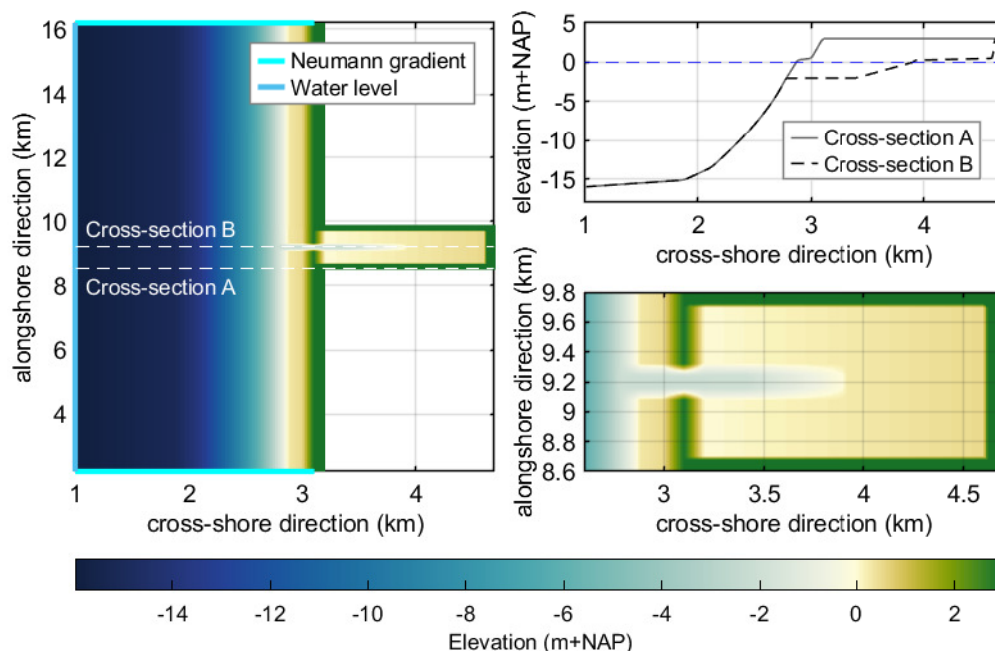


Figure 2.3: Visualization of the schematized bathymetry and model domain. **Left:** Top view of the entire bathymetry. **Top right:** Cross-sections of the domain in the cross-shore direction. **Bottom right:** Top view of model domain with a refined grid cell size of 10x10m.

The managed realignment site is enclosed by dikes. The dikes divide the estuary from the tidal basin reach up to 3m+NAP and back to 0m+NAP over a distance of 200m, where in reality the dikes along the Western Scheldt are much higher (over 9m+NAP). The height of the dike is chosen such that the water level cannot exceed the height of the dike. The newly created wetland behind the dike stretches 1400m in the landward direction and 1000m in the alongshore direction. Its dimensions are roughly based on previously opened wetland restoration projects in the Western Scheldt estuary such as the Perkpolder and the Hedwiges-Prosperpolder. The area has a linearly sloping elevation from 0m+NAP at the estuary side to 0.5m+NAP, promoting drainage during ebb conditions. This represents the typical elevation behind a dike in the Western Scheldt (Weisscher et al., 2022), as well as representing the most natural biogeomorphological development possible. The tidal basin is surrounded by dikes that reach up to 3m+NAP. A cross section of the domain can be seen in Figure 2.3.

The initial inlet dimensions are based on the the well-known empirical relationship for area below mean sea level in relation to the spring tidal prism (O’Brien, 1931, Eq. 2.1). Probably the most widely referenced data set for determining the empirical coefficients is that of Jarrett (1976). Hereof, the empirical coefficients for unjettied inlets (Table 4) are used to determine the area below MSL. The initial spring tidal prism is estimated from a preliminary model run without morphological development, resulting in $P = 3.71 \cdot 10^6 \text{m}^3$. Filling in Eq. 2.1 for the above mentioned coefficients and the tidal prism results in an inlet area below mean sea level ($A_{b,MSL}$) of 222m^2 (Figure 2.4). The inlet is placed in the middle of the managed realignment site and is flat over a width of 80m. It cuts through coastal profile maintaining its shape in the direction of the estuary channel. In the landward direction, bed levels are interpolated between the depth of the inlet channel and the lightly sloping bathymetry of the tidal basin up to half the wetland length. On the sides of the inlet, the bed levels are linearly interpolated between the channel and the pre-existing bathymetry, smoothly integrating it. The number of grid points in the inlet in the alongshore coordinate is 24 at a minimum, far above the number of points needed to resolve key features (Williams & Esteves, 2017), such that inlet dynamics are presented properly.

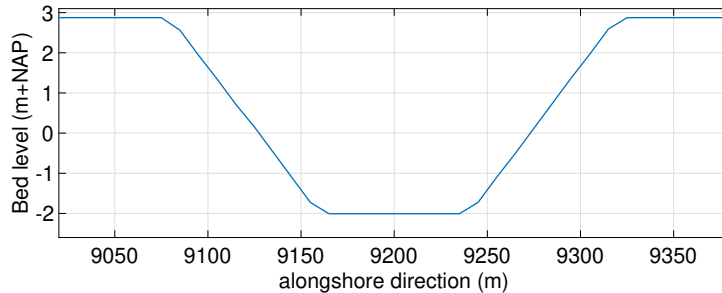


Figure 2.4: Initial bed level of the inlet channel in the middle of the inlet

The grid cell size is 10x10m in the managed realignment site and the near inlet area (Figure 2.3 bottom right). The grid resolution gradually decreases to 40x60m (cross- x alongshore direction) in the top and bottom west corner of the domain. This way the grid in the estuary is directed in the dominant flow direction and the grid resolution remains high in the areas of interest, while limiting computational power. The grid resolution is able to capture the largest channel forming (Best et al., 2018) in the tidal basin as present in salt marshes along the Western Scheldt estuary, while neglecting the smallest spatial scales. A detailed explanation of the grid refinement is given in Appendix A.3

2.3.2 Boundary conditions

The domain is forced by tides only. The river discharge is neglected as it only on the order of 1/1000 of the tidal prism and its contribution to the hydrodynamic activity is minimal. The model contains three open boundaries at the southern, western and northern end of the model domain, while the rest of the model is enclosed by high elevation areas.

A common way of imposing boundary conditions is by forcing uniform water levels based on tidal constituents at the offshore boundary (Best et al., 2018; Braat et al., 2017; Duong et al., 2017; Willemsen et al., 2018). A downside of this approach is that the alongshore flow velocities as a result of the tidal motion are not reproduced. As a consequence, such modelling studies experience artificial infilling of the model domain, as the low flow velocities are not able to mobilize sediments, especially in the absence of waves. An alternative method able to describe the tidal wave travelling in the alongshore direction is presented and explained in detail by Roelvink and Walstra (2005).

Herein, the water level varies over the alongshore boundary, as a result of a phase difference over the length of the boundary. The difference in water level generates a gradient, inducing alongshore flow velocities. The cross-shore boundaries are forced by the water level gradients (Neumann boundary) at the start and end of the alongshore boundary water levels. This method create a more realistic hydrodynamic pattern, which in term can lead to better model performance. Additionally, artificial infilling is counteracted improving estuarine dynamics. A detailed explanation is given in Appendix A.5.

Water levels are imposed on the western boundary (Figure 2.3), representing the M2 and S2 tidal constituents relative to MWL. The values are representative for the Hellegat marsh with an M2 tide of 2.03m, an S2 tide of 0.4M, a spring tidal range of 4.86m and a mean water level 0.18m+NAP (van der Wal et al., 2008). The northern and southern boundary are forced with Neumann boundary conditions (Appendix A.5). For every tidal constituent the phase difference and water level gradient amplitude is calculated (Table 1). The period of the tidal constituents are slightly out of phase, such that a spring-neap cycle is repeated over approximately 14.6 days. The tidal constituents do not align perfectly, but this effect is only minor and not of importance over long periods of time.

		Symbol	Unit	M2	S2
Amplitude	Waterlevel	$\hat{\zeta}_j$	m	2.03	0.4
	Water level gradient	$\partial\hat{\zeta}_j$	-	2.26E-05	4.62E-06
Frequency		ω	rad/h	1.41E-04	1.45E-04
Phase difference		ϕ	degree	8.95	9.26

Table 1: Overview of the values produced by Neumann boundary conditions. Based on the a characteristic water depth of H=16.18m (Minimum bed level + MWL).

2.3.3 Morphodynamic settings

The bed of the Western Scheldt outside of the intertidal wetlands consists of predominantly sand with a median grain size D_{50} of $\sim 200\mu m$. Accordingly, an initial bed of sand with the median grain diameter was used to represent the model domain in agreement with comparable idealized modelling studies (Braat et al., 2017; Weisscher et al., 2022). In reality, a variable mud fraction is present throughout the estuary (TNO, 2019), increasing in the direction of the estuary sides where intertidal wetlands and salt marshes are present. These intertidal wetlands

and salt marshes generally consist of a uniform fine cohesive sediment (Willemsen et al., 2018). Defining a spatially varying sediment composition is possible and would be preferred, but is not implemented due to priorly present model limitations. Sand is supplied at the boundaries as an equilibrium condition, meaning local flow conditions determined the supply rate, which prevents erosion and deposition at the boundaries. Cohesive sediments are supplied as a single mud fraction with a typical dry bed density of 500 kg/m^3 (Deltares, 2022b) and a sediment settling velocity of 0.25 mm/s (Braat et al., 2017). Cohesive sediment is supplied along the estuarine boundaries as a constant concentration of 30 mg/L based on the measured depth averaged values in the stream channel of the Western Scheldt (Temmerman et al., 2004).

The initial sediment thickness is spatially varying and is based on the non-erodible layer as present in the Western Scheldt (Dam, 2013). At the deepest point ($-16 \text{ m} + \text{NAP}$) the initial sand layer is 4 m thick up to a maximum depth of $-20 \text{ m} + \text{NAP}$. The sediment thickness for the rest of the domain is the difference between the maximum depth and the initial bed level. The non-erodible layer also prevents extreme erosion in the estuarine area, which would reduce the validity of the hydrodynamic boundary conditions.

The bed is initiated with the stratigraphic bed module (section A.2). The stratified bed tracks location of sediment in the bed, such that recently deposited sediments erode first, preventing artificial mixing with deep buried sediments. The top transport layer is modelled as a single Lagrangian layer with a thickness of 0.1 m in which sediment exchange occurs with the water column. Below the transport layer are 50 vertically fixed Eulerian layers with a thickness of 0.1 m (total thickness of 5 m) and a single base layer to store bed composition in the vertical (Figure 2.5).

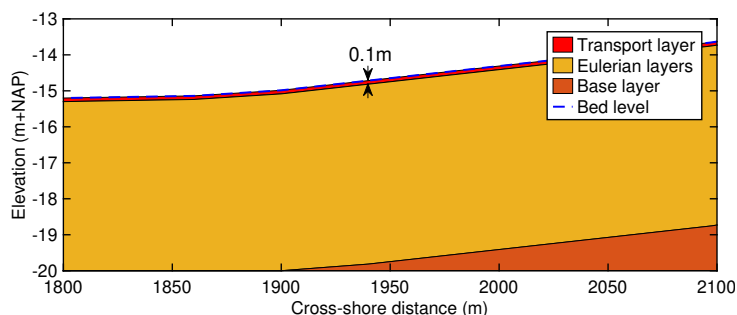


Figure 2.5: Cross-section of the initial bed stratification in the estuarine channel. Single base layer is only present if the thickness of the stratified bed layers is insufficient to store the bed composition.

Table 2: Hydrodynamic and morphodynamic model parameters. A detailed explanation about the choice of model parameters is given in Appendix A.4

Variable	Symbol	Value	Unit	Source
Hydrodynamic				
uniform friction coefficient	n	0.023	s m ^{-1/3}	Deltares (2022a) Wamsley et al. (2010)
Eddy viscosity	ν	0.1	m ² s ⁻¹	Deltares (2022a)
Eddy diffusivity	D	0.1	m ² s ⁻¹	Deltares (2022a)
Maximum timestep	-	15	s	van Dongeren (2018)
Morphodynamic				
Erosion of adjacent dry cells	-	0.5	-	Braat et al. (2017)
Thatcher-Harleman lag time	-	240	min	Best et al. (2018)
Transverse bed slope	α	5	kg m ² s ⁻¹	Baar et al. (2019)
Acceleration factor	MF	100	-	Best et al. (2018)
Specific density	ρ_s	2650	kg m ⁻³	Deltares (2022b)
Mud				
Dry bed density	ρ_{mud}	500	kg m ⁻³	Deltares (2022b)
Settling velocity mud	w_s	0.25	mm/s	Braat et al. (2017)
Critical bed shear stress for erosion	$\tau_{cr,e}$	0.5	N m ⁻²	Willemsen et al. (2018)
Critical bed shear stress for deposition	$\tau_{cr,d}$	1000	N m ⁻²	Deltares (2022b)
Erosion parameter	M	1*10 ⁻⁴	kg m ² s ⁻¹	Braat et al. (2017)
Sand				
Dry bed density	ρ_{sand}	1600	kg m ⁻³	Deltares (2022b)
Median grain size sand	D ₅₀	200	μ m	Braat et al. (2017)

2.4 Model validation

Simulated hydrodynamics and morphology were compared to a combination of empirical formulas and field data to gain confidence in the models ability to reproduce Western Scheldt characteristics. The goal of the validation is not recreate exact values, but determine if the proposed values are within an acceptable range.

Hydrodynamic

Hydrodynamics were validated by comparing the simulated peak flow velocities versus depth below high water level (HWL) against a previously calibrated model of the Western Scheldt (Verbeek et al., 2000). Peak flow velocities were obtained from a regression analysis based on the calibrated model (Leuven et al., 2018), which showed good correlation ($R^2=0.73$) between the peak flow velocities and the depth below high water level. Comparing flow velocities determines whether the alternative boundary conditions are able to reproduce the motion of the tidal wave propagating through the estuary.

Morphodynamic

Morphodynamic validation is performed by comparing accretion rates (below) and inlet evolution (Section 2.5). The accretion rates from managed realignment sites with similar hydrodynamic characteristics are listed in Table 3.

Table 3: average accretion rates of comparable MR sites. The Perkpolder has an accretion rate for the total area (Tot) and area with a bed level above 0.5m+NAP (>0.5). MHWT = mean high water tidal prism.

Location	Average rates (cm/year)		months	MHWT (m) Approx	Source
Perkpolder (NL)	6 (Tot)	3.2 (>0.5)	10	5	Brunetta et al. (2019)
	4.8 (Tot)	2.6 (>0.5)	20		
Tollesbury (UK)	3.3		22	5	Cousins et al. (2017)
Langenhoe (UK)	6		22	5	Cousins et al. (2017)

2.5 Inlet evolution

The inlet connecting the tidal basin to the estuary is subject to change under the influence of the different hydrodynamic and sediment characteristics. Correctly predicting inlet dimensions and development is important as this can influence the hydromorphological development of a MRS (Friess et al., 2014; Townend et al., 2010). Below, the methods for determining its shape and dimensions are elaborated. It describes the most general conception of determining the equilibrium inlet area by means of an empirical relationship (from here: ER) (Section 2.5.1). In addition, a not so common more physical based analytical approach is introduced (Section 2.5.2), called the regime channel method (from here: RCM). The performance of the regime channel method is evaluated by comparing the calculated and measured inlet dimensions of the recently opened Perkpolder, a managed realignment site in the Western Scheldt (Section 2.5.3)

2.5.1 Equilibrium relationships

A general conception in a number of studies determining inlet dimensions is that they tend to some equilibrium area below mean sea level over time in relation to their spring tidal prism (Byrne et al., 1980; Hume, 1991; Jarrett, 1976; Townend, 2005). This well-known empirical relationship for the equilibrium cross-section based on tidal prism, first developed by O'Brien (1931), is in its general form given by:

$$A = CP^q \quad (2.1)$$

where A (m^2) is the cross-sectional area (relative to the mean sea level) and P (m^3) is generally the spring tidal prism passing through the inlet. C and q are the empirical parameters calculated from real world inlets. In general, these inlets reach some form of equilibrium based on phenomenological similarity (Stive et al., 2011) ensuring:

1. similar tide characteristics (form number, amplitude);
2. similar grain size and density;
3. similar wave driven littoral drift;
4. similar shape of cross section.

Multiple equilibrium inlet empirical coefficients (Table 4) will be compared against the inlet evolution of the MRS. These coefficients range from well-known to systems with similar phenomenological characteristics with respect to the MRS. Looking closely at such relationships reveals that, even within systems with similar phenomenological characteristics, the confidence limits wherein these relationships lie can predict cross-sectional areas that lie an order of magnitude apart.

The limited applicability of such relationships, the significant range of values they can produce and the inability to include information about site conditions means that this approach has limited practical use in the design and development of a managed realignment breach. This is especially true for a managed realignment breach, as its positions in the tidal frame, dimensions and shape do not occur naturally.

Table 4: empirical coefficients for inlet equilibrium relationships. Additional info refers to the within paper notation of the relationship.

Source	C	q	Additional info
Jarret(1976)	3.8E-05	1.030	unjettied
Byrne(1980)	8.08E-03	0.64	Chesapeake + Mayor-Mora
Hume (1991)	4.37E-04	0.915	no causeways
Townend (2005)	4.00E-04	0.913	NZ & UK: type C

2.5.2 Regime channel method

A more physically based analytical approach determining breach dimensions based on local hydrodynamics, sediment characteristics and site hypsometry called the regime channel method (RCM) is presented in Townend (2008). The RCM for deriving inlet dimensions is based on the mass continuity equations describing the transport of water through the inlet, wherein the volume of water flowing through the inlet is equal to the volume of water in the MRS. The mass continuity is combined with calculating the hydraulic depth based on a regime channel. The calculations are performed for different tidal stages corresponding to a certain water level, inundated site surface area and vertical velocity. For every tidal stage a parabolic cross-section is calculated based on a design approach proposed by Cao et al. (1997). The resultant channel is taken as the superposition of all parabolic cross-section based on the maximum depth along the width of the channel (Figure 2.6). A more thorough explanation can be found in Section B and the original research paper by Townend (2008). Note that the RCM describes the shape and dimensions of the inlet for the entire tidal prism, while the inlet area below MSL is taken as a measure of comparison with the empirical formulations.

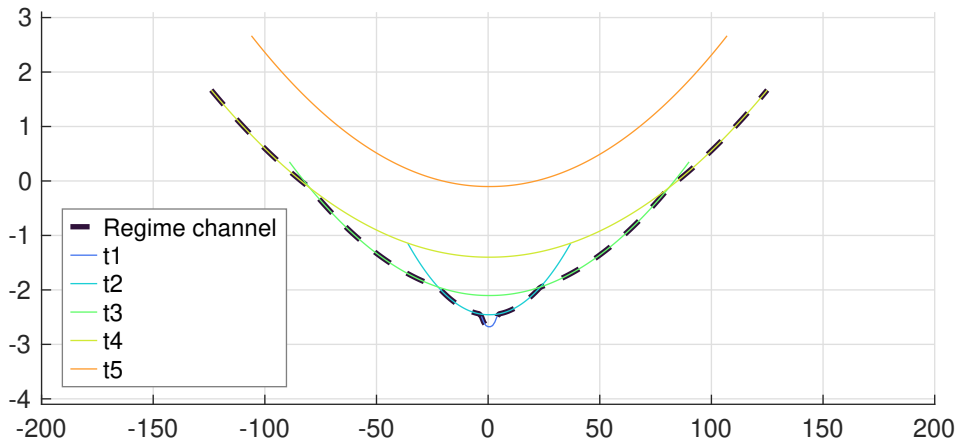


Figure 2.6: Example of the regime channel method construction. t1-5 represent the parabolic shaped design channel for different water levels and regime channel the bounding envelope of the superposition of parabolic cross-sections.

2.5.3 Inlet dimensions performance

Before application, the regime channel method was compared to the inlet evolution of a managed realignment site in the Western Scheldt called the Perkpolder (Figure 2.1). Since June 2015 the Perkpolder is opened along a transect of 350m in the Northeast corner. It is located upstream of the Hellegatpolder and features similar phenomenological characteristics. The dimensions of the Perkpolder are approximately 700m in the crossshore direction and 1200m in the alongshore direction.

The hydrodynamic conditions are comparable with those of the Hellegatpolder, with an average tidal range of 4.6m, a mean sea level of 0.18m+NAP and a spring tidal range of 6.0m (de Wilde, 2022). Winds are coming predominately from the southwest (de Wilde, 2022), sheltering the Perkpolder from wind waves. For the use of the RCM a typical spring tidal range is extracted from water level data at Walsoorden (RWS, 2023b), creating a sinusoidal shape with the water levels between -2.5m+NAP and 3.0m+NAP over a duration of 6 hours.

Sediment characteristics throughout the Perkpolder are spatially heterogeneous with a median grain size $D_{50} = 45\mu m$, but grain size increases in the direction of the inlet with a maximum median grain size of $150\mu m$ corresponding to fine sand (de Wilde, 2022). For the calculation of the inlet area below MSL by the regime channel method, two sediment fraction will be compared. A silt sediment fraction with a median grain diameter $D_{50} = 64\mu m$, slightly higher than the median grain diameter of the inner basin as the median grain diameter is rising towards the inlet and a sand sediment fraction with a median grain diameter $D_{50} = 150\mu m$. The bathymetry of the Perkpolder is derived from combining yearly LIDAR measurements (RWS, 2023a) and multi-beam measurements (Table 5).

Table 5: Performed measurements at Perkpolder in the period 2015-2024

Measuring equipment	Resolution	date	Frequency
Lidar	2m x 2m	2015-2024	1 /yr
Multi-beam	1m x 1m	2015-2025	4 /yr

2.6 Data analysis

Model scenarios are run to determine the effect of physical forcings and design choices on morphological development. Herein, the total accretion is of interest, as a the success of a NbS solution for either nature restoration or flood safety is largely dependant its ability to vertically accrete. In addition, a more normalized approach is introduced as not all scenarios are under the influence of the same physical forcings and comparing the total accretion rate can a give skewed view of the results. Therefore, the trapping efficiency is introduced. The trapping efficiency calculated the total accretion rate as a percent of the total sediment that flows into the basin, such that the effect of different physical forcings are diminished. The trapping efficiency is of interest, as it can tell something about the ability of a system to accrete even under less preferable circumstances.

2.7 Model scenarios

After opening, a typical timescale for geological restoration can be in the range of 15-60 years (Gerwing et al., 2020). van Belzen et al. (2021) reported a time span of 30-50 years for managed realignment sites to reach the desired height, where pioneering vegetation could start after

25 years. The run time of the model (25 years) is chosen such that the typical infilling and adaptation to the opening is taken into account, but the implementation of a vegetation module is not necessary. The different scenarios are based on changes in external forcing and wetland configuration.

The first set of scenarios are focused on physical drivers of hydromorphological development. The tidal constituents determine the hydrodynamic forcing and sediment availability determines the ability to accrete. Two scenarios with different tidal constituents are simulated consisting of a single M2 (with an amplitude of 2.03m) tide and the combination of an M2S2 tide (amplitude of 2.03m + 0.4m). The suspended sediment concentrations (SSC) imposed at the boundary are 30mg/L, 50 mg/L and 70mg/L. Although the latter two suspended sediment concentrations are relatively high for the location of the Hellegatpolder (Temmerman et al., 2004), such values are not uncommon further upstream in the Western Scheldt.

Management realignment projects are anthropogenic, thus subject to design choices that can be made to reach the desired goal of the project. The second set of scenarios focuses on the influence of design choices on the hydromorphological development. An important feature controlling the flow and transportation of sediment is the inlet. The inlet approach as explained in Section 2.5.2 is used to determine the initial inlet area and shape, in order to determine the influence of breach dimensions closer to equilibrium. The second design choice is the dimensions of the area. The dimensions may influence the total accretion rate and are, from an estuary wide perspective, important when the managed realignment sites objective involves flood protection (Pontee, 2015; Townend, 2008; Weisscher et al., 2022). The alongshore dimensions in both the down- and upstream direction are doubled, while the cross-shore dimensions remain equal. Herein, the inlet dimensions are altered based on Jarrett (1976), while maintain the width to depth ratio.

Table 6: Overview of morphodynamic scenarios. *Sediment concentration scenarios are ran with M2 tidal constituent only.

Scenario	Description
S1	
a	Reference scenario
b	Only ran with M2 tidal constituent
c*	SSC = 50mg/L
d*	SSC = 70mg/L
S2	
a	Inlet area based on the RCM (Townend, 2008)
b	Area increased to 2000x1400m

3 Regime channel method performance

The Perkpolder MRS was breached along a 350m wide transect to create an inlet. The morphodynamic evolution of the inlet is described in this section. In addition, the inlet evolution based on the RCM is calculated based on they hydrodynamic and morphological characteristics of the Perkpolder. The inlet area below MSL of both methods is compared in order to verify the use of the regime channel method under different hydrodynamic and morphological characteristics as present in the original paper by Townend (2008).

3.1 Measured inlet development Perkpolder

To analyse the morphodynamic development of the inlet, the bathymetry of the Perkpolder (Figure 3.1) is derived by combining the LIDAR and multi-beam measurements. When overlapping, the multi-beam data is leading, as these measurements are carried out for the Perkpolder specifically. To analyse the morphodynamic development of the inlet, two transects are considered as shown in Figure 3.1, in order to determine whether spatial differences along the inlet are present. The first one is the shortest path between the top of the remaining dike and the second follows the path of the old dike.

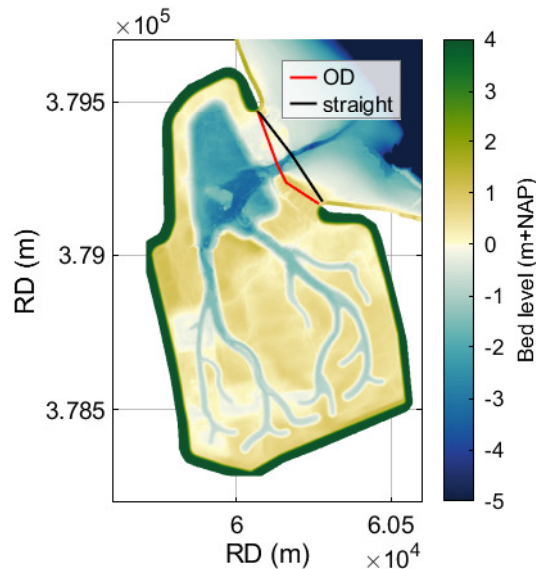


Figure 3.1: Bathymetry of the Perkpolder in 2016. two transects for inlet development. A straight transect and a transect that follows the old dike (OD)

The evolution of the inlet area below MSL is shown in Figure 3.2. The inlet erodes rapidly in the first year and kept eroding at a slower rate in the years after. after the first few months of 2020 the inlet area below MSL is stabilizing. The direction of change in inlet area below MSL is the same for both transects, where the 'old dike' transect has slightly lower values. This is mostly due to the fact that the maximum depths along this transects remain higher (Figure 3.3), creating a more efficient channel and thus lowering the total flow area. This effect diminishes over time as the inlet develops to an equilibrium over time. However, equilibrium is not yet reached, as the inlet area should decrease due to infilling of the MRS.

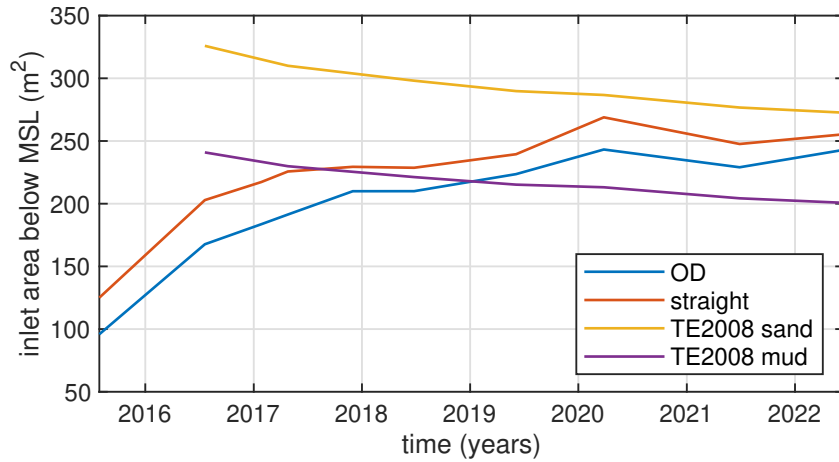


Figure 3.2: Area below MSL of the Perkpolder MRS and as calculated with RCM of Townend (2008). **OD**: Old dike, **straight**: shortest transect length

The inlet shape for both transects over time is shown in Figure 3.3. Both transects erode, creating a small and deep channel. The straight transect deepens very quickly, climaxing in 2017 and shallowing after. As the inlet area below mean sea level is still rising during this period (Figure 3.2) erosion takes place on the sides of the channel. In the downstream direction a shallow but broad secondary channel is created, while in the upstream direction erosion occurs as elongation of the main inlet channel. For the old dike transect, erosion divides the main channel in two, where the upstream part quickly stabilizes and the downstream part erodes deeper and only starts to shallow slightly after 2020. Erosion on the sides of the inlet create a very shallow secondary channel in the downstream direction. In the upstream direction inlet erosion takes place close to main channel, but bed level changes further upstream do not change much. As the inlet area is below equilibrium, the same tidal prism has to pass through it for a smaller surface area, increasing flow velocities and scouring the inlet. Scouring deepens the inlet significantly during the first years after opening (lowering the width/depth ratio). A deeper channel is more efficient and a smaller flow area may be required for any tidal prism.

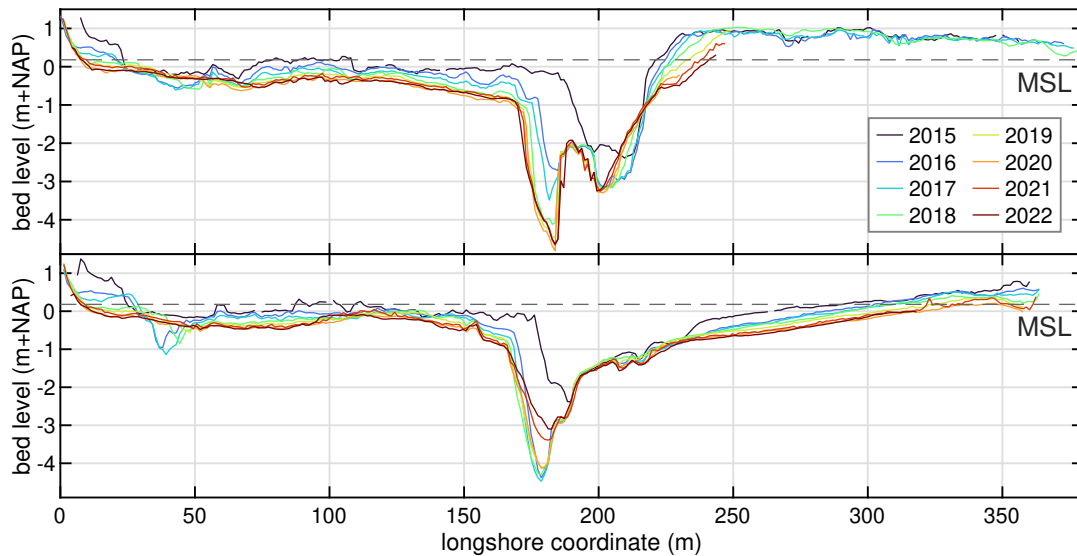


Figure 3.3: Inlet development of the Perkpolder MRS over the period 2015-2022 for the two transects shown in Figure 3.1. alongshore coordinate 0 = downstream and alongshore coordinate max = upstream. **top**: Old dike transect and **bottom**: straight dike transect

3.2 RCM for the Perkpolder

The RCM is based on the critical shear stress for erosion of the present sediment fraction in the MRS inlet area. The inlet dimensions are calculated for two sediment fractions representing the heterogeneous sediment composition in the inlet. Herein, the critical shear stress for erosion of mud $\tau_{cr,m} = 0.5\text{N/m}^2$ (van der Vegt et al., 2021). The critical shear stress of sand is based on Soulsby (1997), resulting in $\tau_{cr,s} = 0.141\text{N/m}^2$. However, the critical shear stress of sand is increased in the presence of mud (van Ledden, 2003) which is abundantly present in the Perkpolder MRS. Therefore, the critical shear stress of sand is adapted by equation A.2 such that the critical shear stress of sand for erosion is doubled, resulting in $\tau_{cr,s} = 0.282\text{N/m}^2$. The development of the inlet area below MSL as calculated with the RCM can be seen in Figure 3.2.

Initially the inlet area is very large, shrinking as the Perkpolder is filled with sediment. The reduction in inlet area is large at first as accretion rates in the Perkpolder are higher at first and diminish over time as the accretion rate in the Perkpolder diminishes. The inlet area below MSL as measured in the Perkpolder MRS is within the limits of the RCM after approximately 4 years for both transects. This is around the same time as the highly dynamic behaviour of the inlet ends and a more stable equilibrium inlet area is reached. The RCM is thus fairly good at predicting the equilibrium area below MSL for a MRS in the Western Scheldt. It remains to be seen how the inlet area develops further and if the RCM remains applicable to determine the long-term development. This is highly dependant on the sediment composition of the inlet area (Figure 3.2).

4 Results

4.1 Hydromorphological model performance

4.1.1 Hydrodynamic validation

The hydrodynamic boundary conditions reproduce the motion of the tidal wave propagating through an estuary. Peak flow velocities are reproduced well. The RMSE(=0.09 < 0.1 m/s) is good and unbiased (Bias=0.01 < 0.1) according to the statistical guidelines for validation of estuarine models according to Williams and Esteves (2017). The model underestimates flow velocities slightly for low water depth and overestimates them for higher water depths. However, Leuven et al. (2018) states that the regression line is not able to capture the highest flow velocities possible, indicating that the overestimation is in line with previously calibrated models of the Western Scheldt. It should also be noted that the effect of estuary characteristics (e.g. funneling shape of the Western Scheldt) are not reproduced by the model.

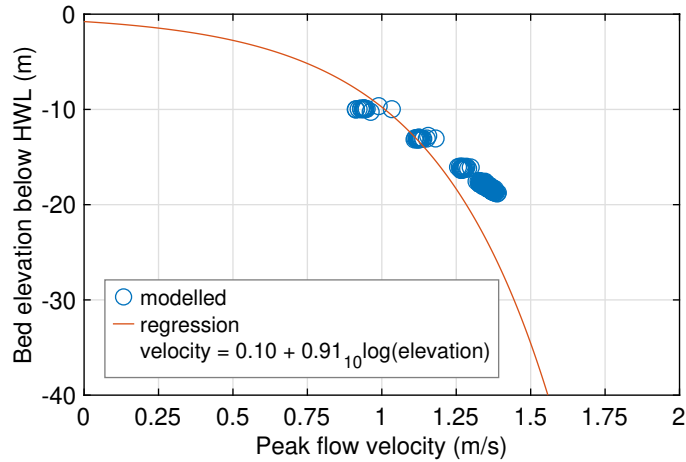


Figure 4.1: Peak modelled flow velocities versus regression line of calibrated 2DH model of the Western Scheldt (regression line retrieved from Leuven et al., 2018)

4.1.2 Morphological validation

The hydromorphological model performance is assessed further by comparing the simulated inlet development to the previously validated regime channel method (Section 3) and several empirical relationships (Table 4). The morphodynamic evolution of the inlet is calculated along a transect in the middle of the dike in the along-shore direction (Figure 4.2).

Before comparison, the regime channel method (for detailed information see Appendix B) is used to calculate the inlet dimensions based on the simulated hydrodynamic and morphological development of the managed realignment site. Herein, a similar approach is used as presented in Section 3.2. The critical shear stress for erosion of mud $\tau_{cr,m}=0.5\text{N/m}^2$ (user-defined), and of sand $\tau_{cr,s}=0.155\text{N/m}^2$ (based on Soulsby, 1997). However, from Figure 4.3 it can be seen that the critical shear stress for erosion is, to some extent, always under the influence of mud. Accordingly, the critical shear for erosion of sand is doubled in the calculations of the inlet area below MSL by the regime channel method resulting in $\tau_{cr,s}=0.341\text{N/m}^2$.

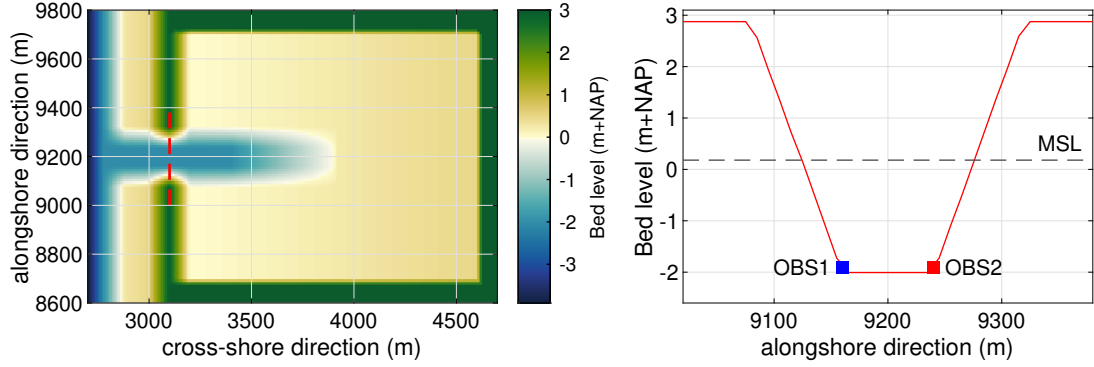


Figure 4.2: **left:** Initial basin bathymetry with location of inlet transect (dashed red line). **right:** Geometry of initial basin inlet along the inlet transect with observation points (red and blue square)

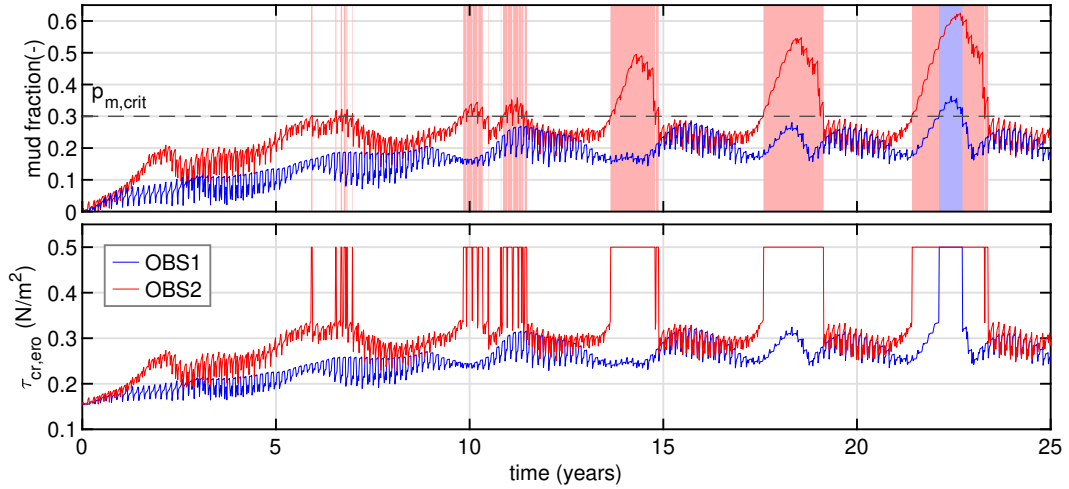


Figure 4.3: **top:** Mud content in the transport layer at 2 observation points in the inlet. Shaded areas show the times where $p_m \geq p_{m,cr}$ and τ_{cr} is governed by $\tau_{cr,m}$. **bottom:** critical shear stress for erosion for corresponding mud content.

Comparison of the inlet area below MSL for the different A-P relationships and the RCM is shown in Figure 4.4. In the short term, the A-P relationship of Hume (1991) comes closest, but still under predicts the inlet area below MWL. For the long-term, none of the A-P relationships are capable of predicting inlet dimensions. The RCM produces bounds based on the two sediment fractions. The modelled $A_{b,MSL}$ is situated within these bounds, providing the best prediction of the long-term development of the inlet.

The bounds produced by the regime channel method resemble a confidence interval. After 20 years of morphological development the tidal prism $TP = 3 \cdot 10^6$ and the confidence interval $CI_{RCM} = 136m^2$. Calculating the equilibrium inlet area below MSL for the same tidal prism within the 95% confidence interval as presented in Jarrett (1976) results in $CI_{jar} = 652m^2$. The RCM thus better predicts the long-term development and narrows the range of values possible for the equilibrium inlet area below MSL.

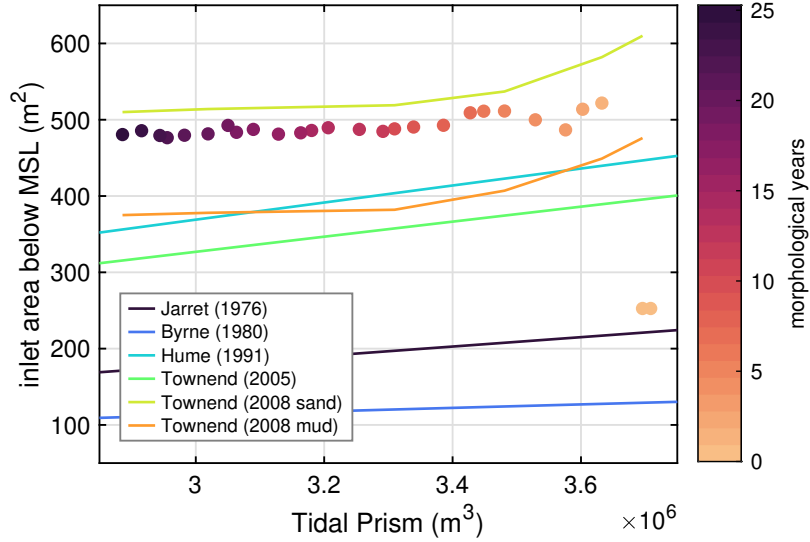


Figure 4.4: The change in P and A in the inlet over time. Herein, the dots represent $A_{b,MSL}$ over time during the model simulation (the jump represents the initial dynamic situation in the inlet).

The accretion rates of the model are compared to several other managed realignment sites with comparable hydrodynamics (Table 7). modelled accretion rates are in good comparison with the evaluated MRSs. The accretion rates of the model are higher than those of the Perkpolder above 0.5m+NAP. Initially, the bed of the model lies lower in the tidal frame (between 0-0.5m+NAP), increasing the hydroperiod and possible accretion. The total accretion rates of the Perkpolder is much higher, which is mostly caused by the large pond that acts as a sediment sinkhole accreting up to 50cm/year in some locations (van de Lageweg et al., 2019).

Table 7: average accretion rates of comparable MR sites. The Perkpolder has an accretion rate for the total area (Tot) and the area with a bed level above 0.5m+NAP (>0.5). MHWT = mean high water tidal range.

Location	Average rates (cm/year)		months	MHWT (m)	Approx	Source
Perkpolder	6 (Tot)	3.2 (>0.5)	10	5		Brunetta et al. (2019)
	4.8 (Tot)	2.6 (>0.5)	20			
Tollesbury (UK)	3.3		22	5		Cousins et al. (2017)
Langenhoe (UK)	6		22	5		Cousins et al. (2017)
Model	4.4		12	4.5		
	3.1		24			

4.2 Hydrodynamics

Maximum flow velocities are higher during flood than during ebb, creating a flood dominant current in the estuary channel (Figure 4.5). The maximum flow velocities occur an our after the maximum change in water level, indicating some lag time.

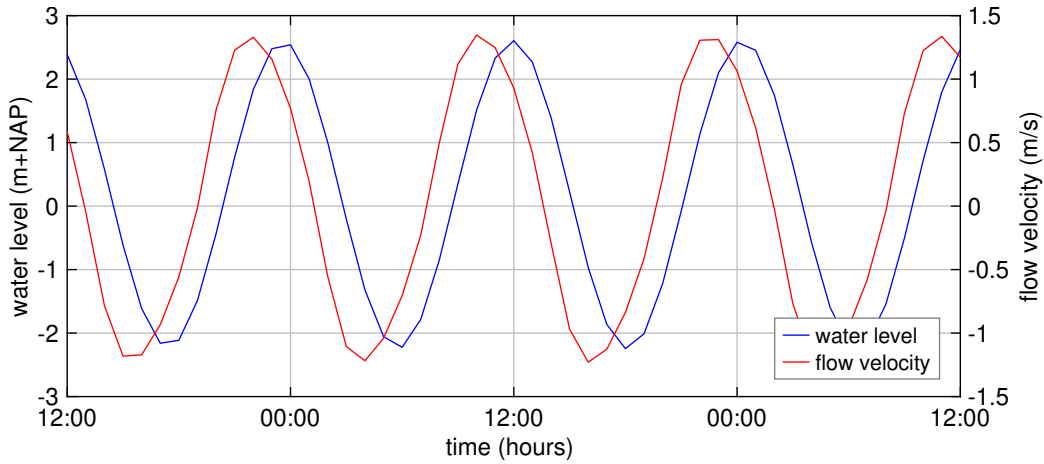


Figure 4.5: Water level and flow velocities in the middle of the estuary channel at $x=1880$; $y=8800$ between 14-nov 12:00 and 16-Nov 12:00.

The water levels in the managed realignment site follow the the water levels from the estuary by the short basin principle (Bosboom et al., 2021). The flow velocities through the inlet are shown in Figure 4.6. The peak flow velocities over the transect are higher during flood, resulting in a flood-dominant current through the inlet. However, the flood dominance is not uniform over the length of the transect. Peak flow velocities in the upstream direction (OBS2) are higher during flood in line with the transect, but peak flow velocities in the downstream direction (OBS1) are higher during ebb. The flood dominant flow velocities from the estuary in the upstream direction are transferred to the upstream side of the inlet and vice versa.

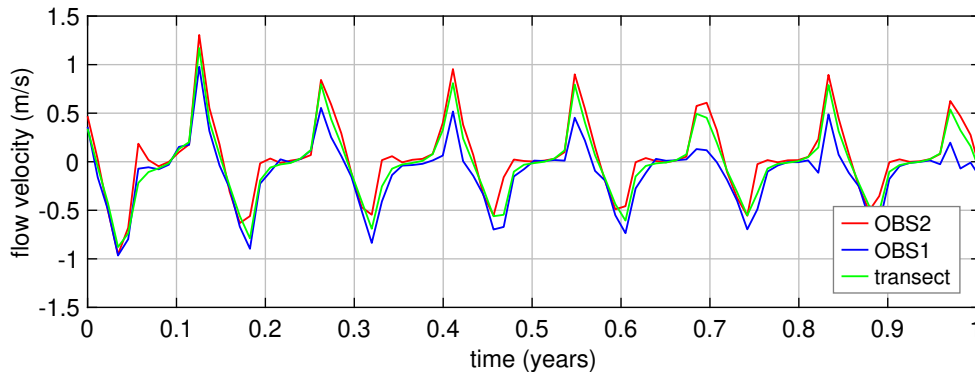


Figure 4.6: Flow velocity in the inlet for the first morphological year along the transect and both observation points from Figure 4.2

4.3 Opening a tidal basin

Below, the results of the reference simulation are shown and described. The morphological development can be divided into three main subsystems, namely, the managed realignment site itself, the inlet and the frontal inlet area. The estuary itself is discussed as a separate system. After, the influence on one another is assessed to describe the interplay of the whole system.

4.3.1 Inlet dynamics

Dimensions

After opening, the initial inlet dimensions change, tending to some dynamic equilibrium under the influence of hydrodynamic and sediment characteristics. The development of the inlet area below MSL along three cross-sections (to check for spatial variability) is shown in Figure 4.7. During the first year of morphological development the area below MSL quickly rises, indicating that the initial inlet area based on Jarrett (1976) is below the systems equilibrium. As a result, 36648m^3 of sand erodes from the inlet and is redistributed to nearby areas. After the first year, the high dynamic change stabilizes as the inlet adjusts to the phenomenological characteristics of the system. During the remainder of the time frame the tidal prism passing through the inlet reduces (Figure C.2). A smaller tidal prism requires a smaller inlet area, causing the inlet area below MSL to diminish over time (Figure 4.7). During this period the erosion and deposition of sand and mud is $\pm 1000\text{m}^3$ per year, only a fraction of the volume of sand eroded during the first year.

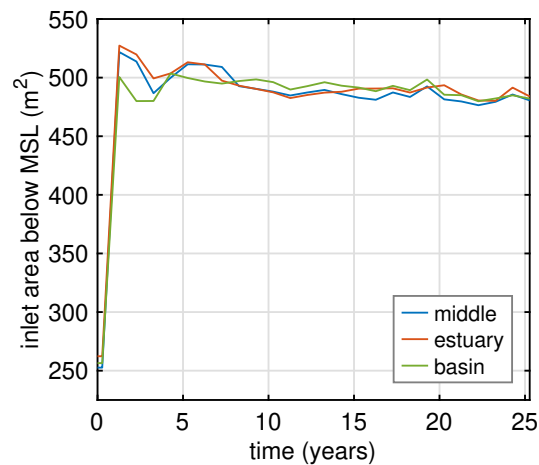


Figure 4.7: Development of the inlet area below MSL over time.

Shape and form

The equilibrium inlet area and its evolution is predicted fairly well. Next, the evolution of the shape and form of the inlet are assessed (Figure 4.8). As the initial inlet area is below equilibrium, the same tidal prism has to pass through the inlet for a smaller surface area. As a result, the flow velocities increase, scouring the bed. Scouring deepens the inlet significantly over the first year of morphological development (lowering the width/depth ratio) and takes a more parabolic shape. A deeper channel is more efficient and a smaller flow area may be required for any given tidal prism. Scouring of the bed is more pronounced in the upstream direction, due to flood dominance of the system (Figure 4.5).

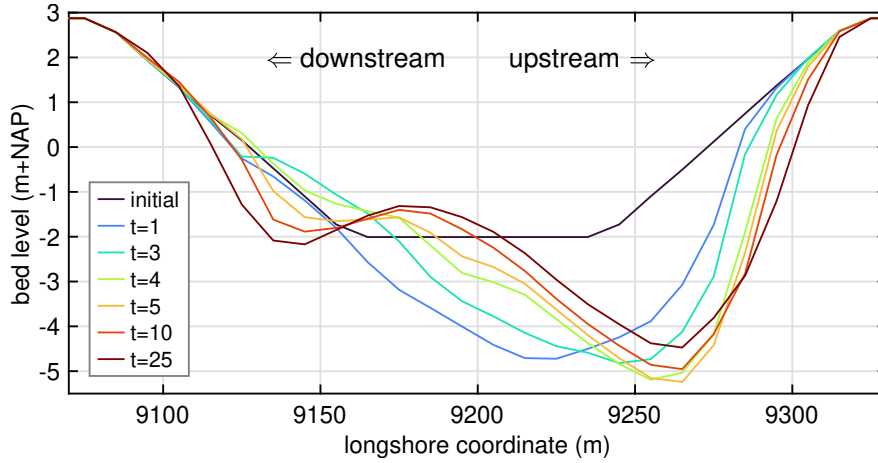


Figure 4.8: Evolution of the inlet shape over 25 years of morphological development

In the upstream direction the main inlet channel continues to deepen and travel in the upstream direction. The maximum depth of the main channel climaxes after 5 years of morphological development. Between 1 and 3 years of morphological development the downstream part of the inlet accretes. After approximately 3 years of morphological development the downstream part of the inlet starts to erode during ebb flow conditions (Figure 4.9), in line with the ebb-dominant peak flow velocities in the downstream part of the inlet (Figure 4.6 OBS1). After 5 years, the main channel starts to shoal, while erosion in the downstream part continues. After 10 years a distinct secondary channel has formed, creating a two channel inlet. During the remainder of the morphological development the shoaling and scouring of the main and secondary channel respectively continued. However, the shape of the channel remains stable after 10 years, indicating that the inlet shape has adapted to local hydrodynamic and sediment characteristics. The final stable shape is vastly different from the shape produced by the regime channel method (Figure 2.6). The initial inlet shape and dimensions thus influence the long-term development of the inlet.

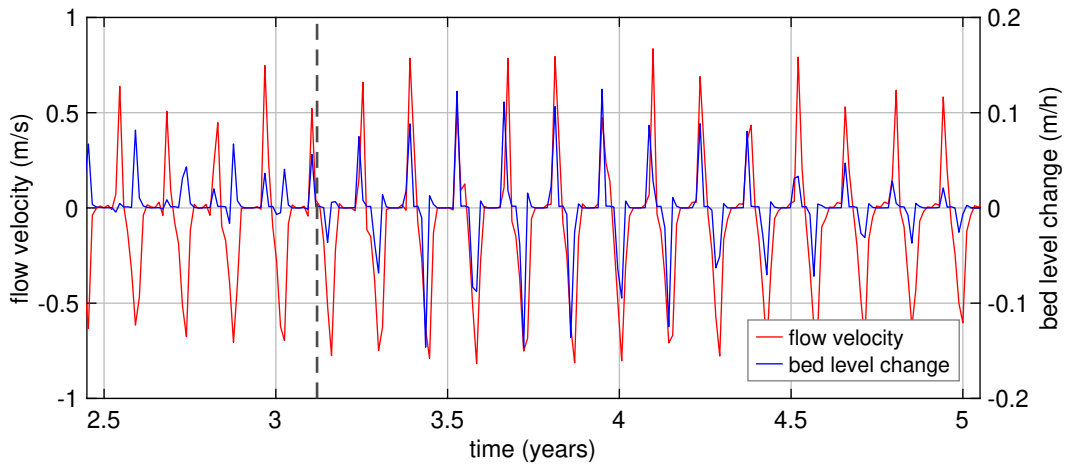


Figure 4.9: Flow velocity and bed level change between 2.5 and 5 years of morphological development at OBS1. Horizontal dashed line indicates the moment when ebb flow velocities cause erosion instead of deposition

4.3.2 Basin dynamics

Next, the morphological development of the managed realignment site is discussed. The accretion rates over time can be found in Figure 4.10. Initially, the accretion rate of sand is high

as a result of the redistribution of sediment from the inlet. After, the yearly accretion rates plummet and vanish almost entirely after 5 years. On the contrary, The accretion of mud is relatively low in the first year and the average accretion rate climaxes after approximately 5 years. As the basin accretes, the tidal prism reduces (Figure C.2) and consequently the hydroperiod. A reduction in hydroperiod reduces the potential time for sediment to settle. As a result, the accretion rates diminish over time as the elevation of the managed realignment site rises relative to the tidal frame.

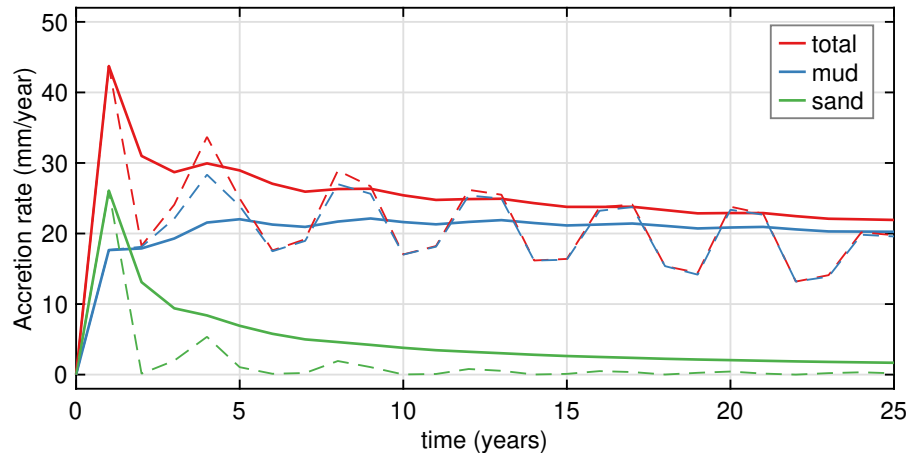


Figure 4.10: **solid line**: Averaged accretion rates w.r.t. opening of the tidal basin. **Dashed line**: represents the non-averaged yearly accretion rates. Accretion rates are averaged to diminish the effect of the spring-neap cycle and the morphological acceleration factor present in the non-averaged accretion rates.

As the initial bathymetry does not include a pre-dug network of channels the first few years after opening are highly dynamic. Moreover, the initial redistribution of inlet sediment adds to the dynamicity of the system. The change in bed level for the first three years of morphological development is shown in Figure 4.11. During the first few years a network of channels develops. The main channels are directed in the landward direction and in the alongshore direction just behind the inlet to promote drainage from the side of the MRS. Interesting to note is the formation of elevated humps of sediment at the sides of the main channel and between the branching channels. The elevation and size of these humps is more pronounced in the upstream direction, as a result of the flood dominant flow that is transferred from the estuary via the inlet to the MRS itself.

The erosion and deposition for the different sediment fractions is shown in Figure 4.12. The formation of the humps is predominantly caused by the redistribution of sand from the inlet and within the basin. During the first year of morphological development the basin accretes $37800m^3$ of sand, very close to the volume of sand that is eroded from the inlet ($-36600m^3$). After the first year, the import of sand is very limited and erosion and deposition patterns are governed by within-site redistribution. After the first year, the import of sand is very limited and erosion and deposition patterns are governed by within-site redistribution. Mud is distributed more evenly across the basin, visible from the lower cell deposition rates with higher basin wide accretion rates (Figure 4.10). During flood, the flow is able to transport cohesive sediment onto the landward end of the basin. Ebb flow velocities at the landward end of the basin are low and not able to resuspend sediment, resulting in the largest deposition rates. Mud deposition is also high in the wake (the side opposite of the inlet) of the large sand humps. During ebb, the sediment transport is directed towards the inlet. The flow is obstructed by the large sand deposits and resuspended cohesive sediment settles as a result. This creates a knock-on effect increasing the elevation of the hump over time.

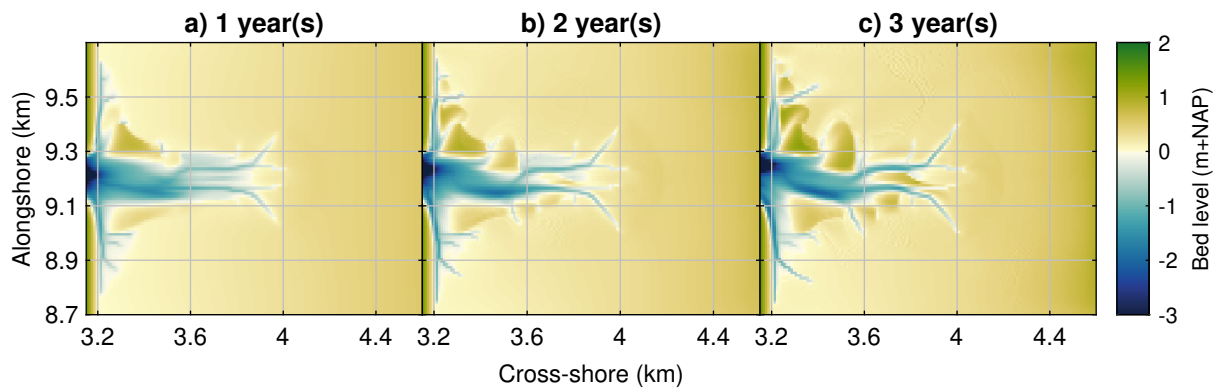


Figure 4.11: Bed level after the after the first three years after opening the MR site

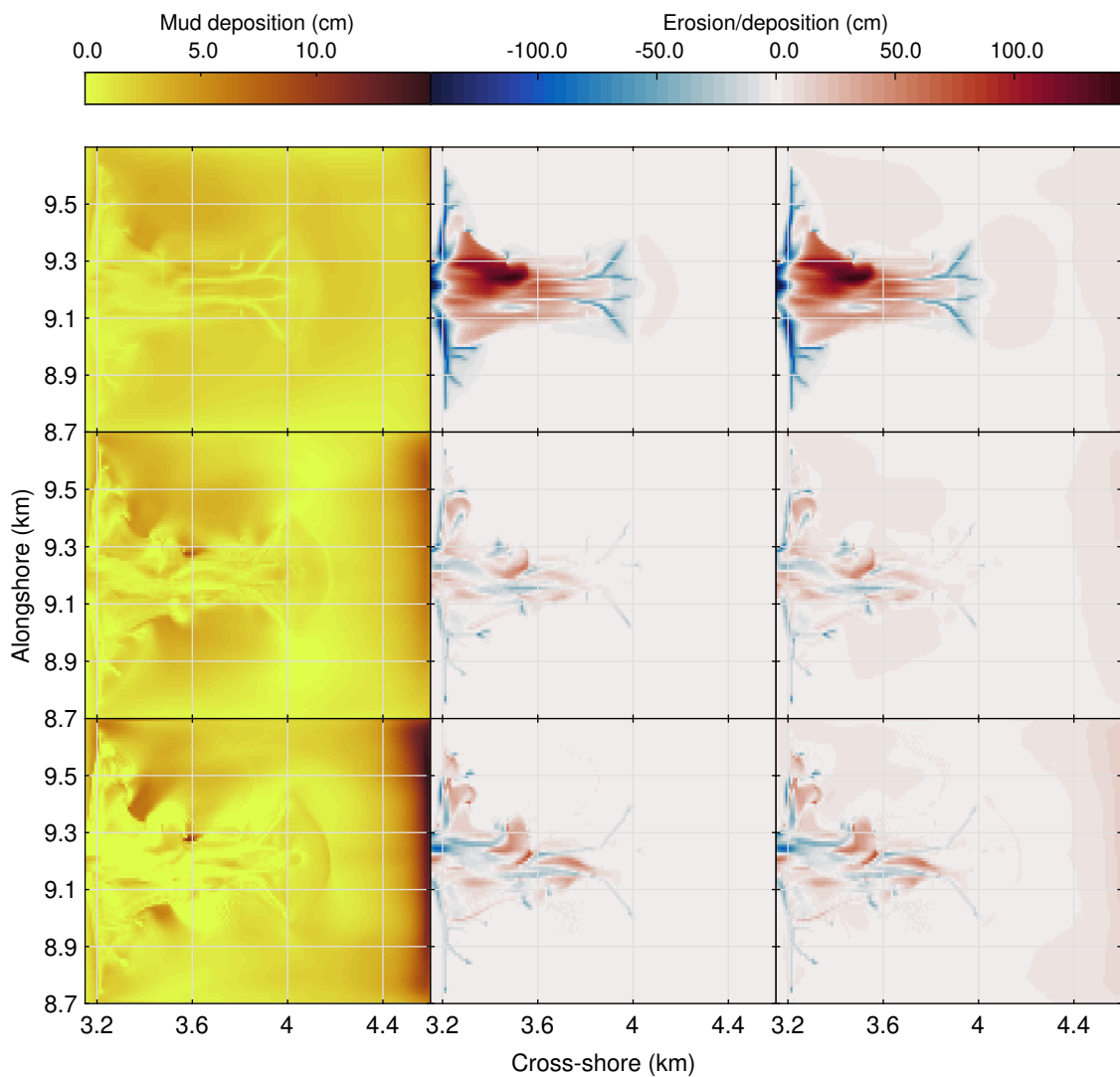


Figure 4.12: Yearly bed level change of the first three years after opening the MR site. **left to right:** Mud deposition, sand erosion/deposition, total bed level change. **top to bottom:** after 1, 2 and 3 years of morphological development.

The result of 25 years of morphological development is shown in Figure 4.13. The basin has two distinct sedimentation patterns. Firstly, the seaward to landward infilling as a results of

cohesive sediments able to reach the landward end of the basin. Hereby, a network of channels that supports the landward transport and drainage of the basin is created within the final bathymetry. Secondly and more interesting, the 'humps' of sediment as a result of the high initial sand deposition that remain. They create high elevated areas in between the channels. These areas have a higher maximum elevation than the landward end of basin. During the 25 years of morphological development their position differs only slightly from their initial position, being pushed away from the inlet. The remnants of the initial sand deposition indicate that initial dimensions of the inlet and basin are important for the long-term development of the basin. A summary of the final erosion and deposition values can be found in Table 8. A greater amount of sand and mud deposition in the upper half of the basin is clearly visible from the total volume changes. The upper half of the basin accretes 34% more over a period 25 years. The dominant flow direction of the estuary is thus of importance to the long-term development of the MRS.

Table 8: Total accretion of sediment and mean bed level change for the MRS after 25 years of morphological development.

	Volume 1000m ³			mean elevation m+NAP		Accretion m
	<i>sand</i>	<i>mud</i>	<i>total</i>	<i>Start</i>	<i>final</i>	
Bot	19.1	321.9	341	0.14	0.77	0.63
Top	41.7	412.0	453.7	0.14	0.61	0.47
Total	60.8	733.9	794.7	0.14	0.69	0.55

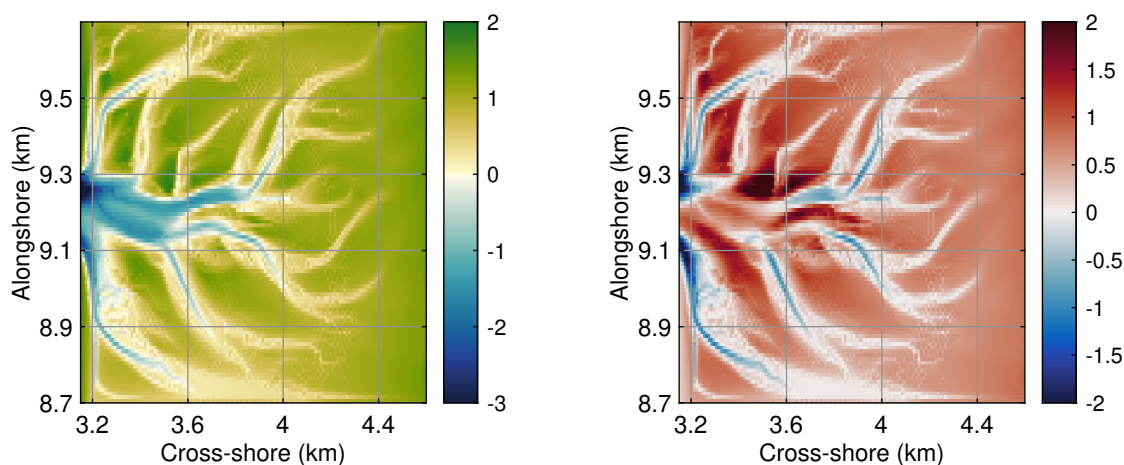


Figure 4.13: morphological development after 25 years **Left**: bed level **Right**: cumulative erosion and deposition of both sediment fraction

4.3.3 Frontal inlet area

The frontal inlet area (FIA) consists of an area, such that the erosion and deposition are clearly under the influence of the tidal motion flowing in and out of the basin. The bed level changes of the frontal inlet area are shown in Figure 4.14. Sand initially erodes from the FIA as it is partly in the extension of the inlet, which heavily erodes. Over the long-term, the initially eroded sand accretes again, resulting in a very small net accretion of sand over the full length of morphological development. Mud is accreting from the beginning elevating the frontal inlet area, reducing over time as higher elevated areas have a smaller hydroperiod.

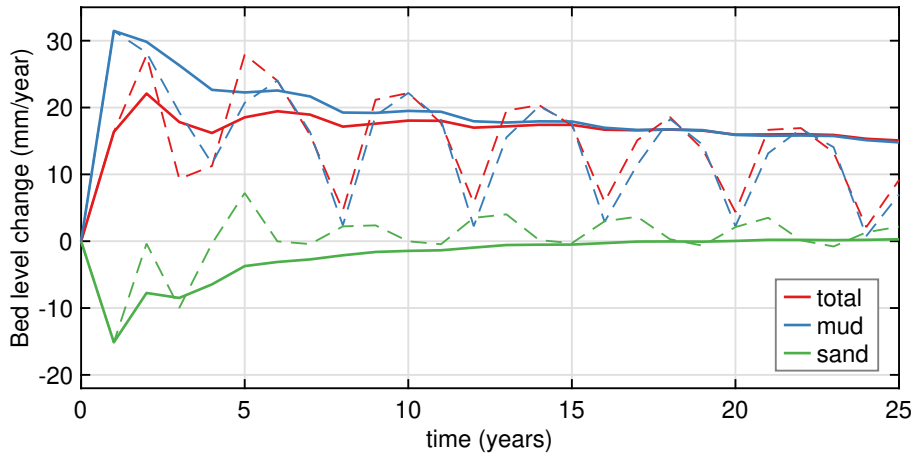


Figure 4.14: **Solid line:** Average bed level change in the frontal entrance w.r.t. opening of the tidal basin **Dashed line:** represents the non-averaged yearly bed level change. Bed level change is averaged to diminish the effect of the spring-neap cycle and the morphological acceleration factor present in the non-averaged accretion rates.

The managed realignment site has a suction effect on the estuary water levels. During flood the rising water level downstream of the inlet is sucked into the managed realignment site. As a result, the flow velocities towards the inlet increase, while slowing down the flow in the upstream direction of the inlet (Figure C.3). The effect of the managed realignment site on the hydrodynamics increases erosion in the downstream direction of the inlet forming a channel (Figure 4.15). In the extension of the inlet a shoal forms due to the reduction in flow velocities, enabling sediment accretion. The erosion and deposition of sand occurs mostly in the extension of the inlet, where the hydrodynamics are under the influence of the managed realignment site (Figure 4.16). Mud settles on the sides of the inlet channel. The diminished hydrodynamic activity in the upstream direction of the channel enhances deposition, while the suction effect erodes the downstream side of the channel. After 25 years of morphological development the frontal entrance area has accreted 2152m^3 and 110928m^3 , resulting in a total sediment import of 113080m^3 .

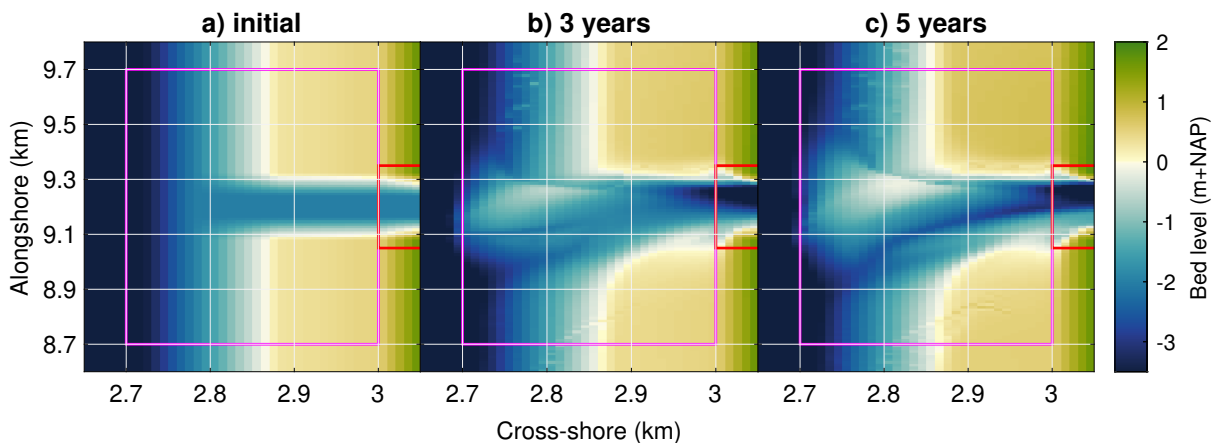


Figure 4.15: Bed level after 3 and 5 years of morphological development. figure is slightly zoomed out for convenience and rectangles present the domain of a subsystem (Pink: Frontal inlet area; Red: inlet area).

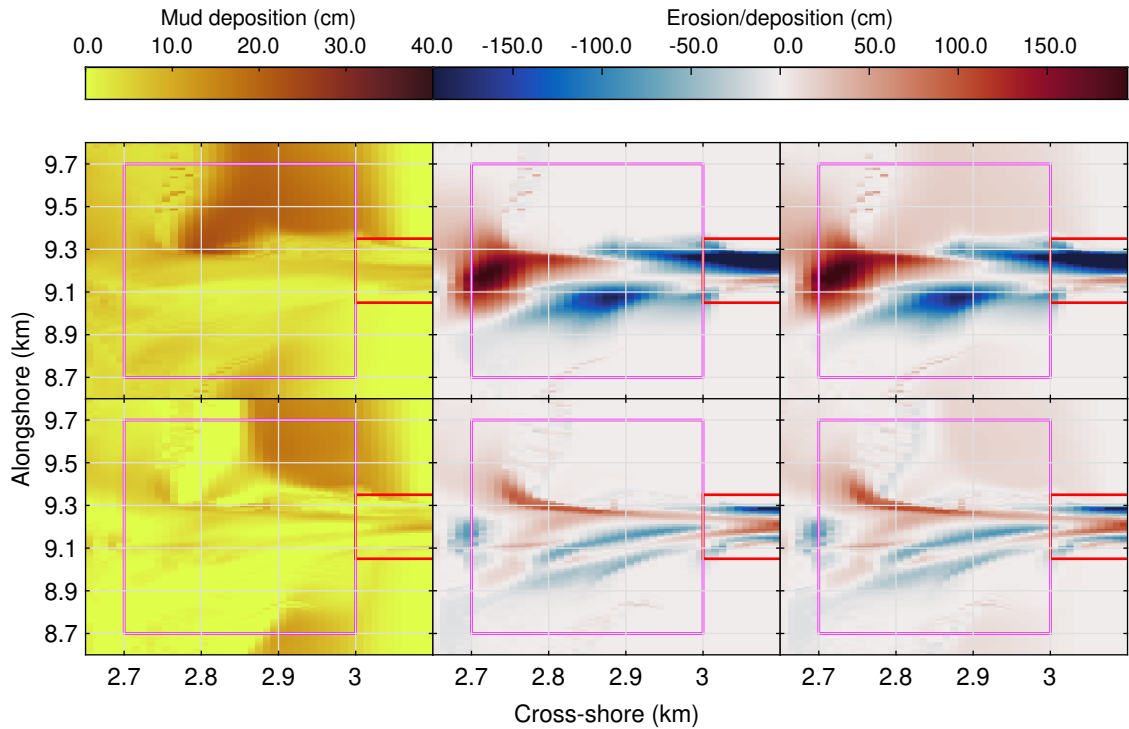


Figure 4.16: Erosion and deposition in the frontal inlet area. **left to right**: Mud deposition, sand erosion/deposition, total bed level change. **top**: between 0-3 years and **bottom**: between 3-5 years of morphological development. figure is slightly zoomed out for convenience and rectangles present the domain of a subsystem (Pink: Frontal inlet area; Red: inlet area).

4.3.4 Estuary

The hydrodynamics of the estuary channel are altered by the opening of the MRS. The MRS sucks in additional water during flood and empties during ebb, increasing necessary drainage capacity. Here, the estuary channel morphology will be analysed. This will be done by introducing a model run without opening of a MRS and comparing the morphological development with the reference model run.

The bed level after 25 years of morphological development can be seen in Figure 4.17. A large shoal forms on the western boundary. This is a model artifact and further discussed in Section C.1. Apart from the shoal formation, the effect of the MRS is clearly visible from the differences in bed level. These are characterized by alternation of deposition and erosion between 1500m and 2500m in the cross-shore direction over the alongshore length. At the downstream end the increased hydrodynamics increase the transport of sediment through the boundary. Moving to the north up until the start of the MRS an area of increased erosion is situated. The suction effect of the basin is clearly visible, as the increased hydrodynamic activity alters the sediment transport. North of the MRS an area of increased deposition is visible, as a result of the decreased hydrodynamic activity in the upstream direction of the MRS. The MRS has an eroding and depositional effect on the estuary based on location relative to the inlet.

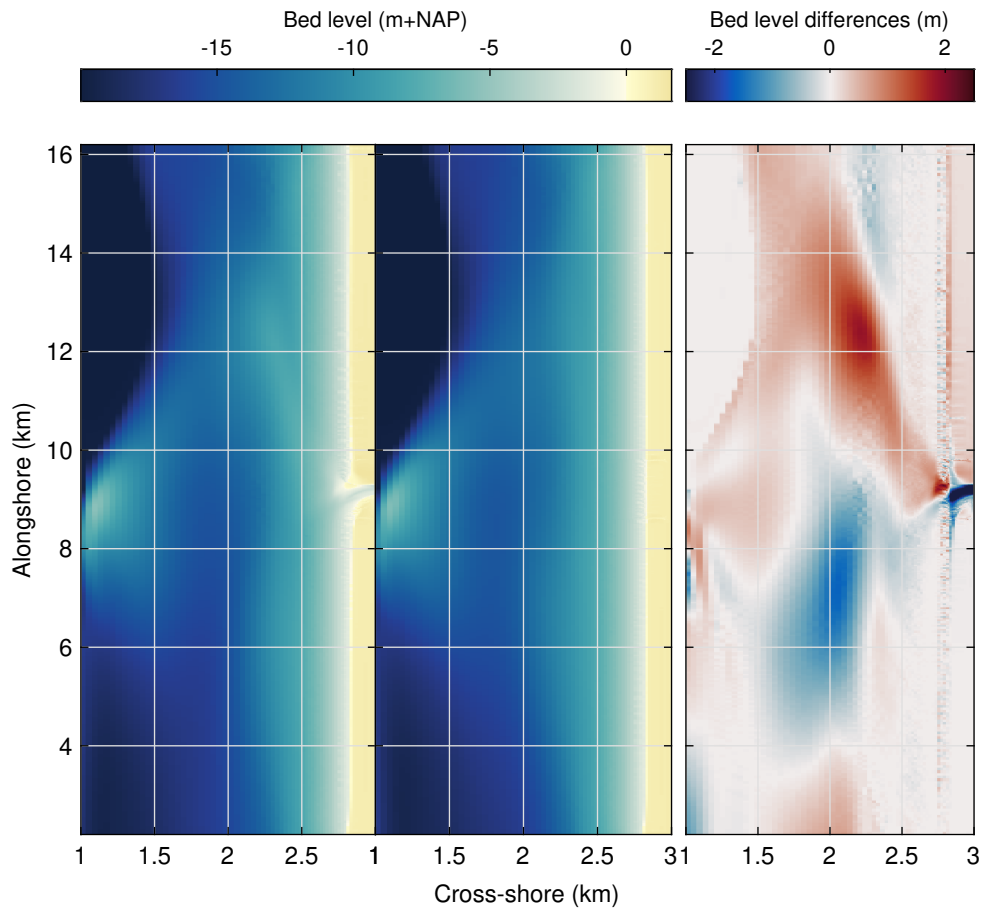


Figure 4.17: Bed level after 25 years of morphological development for the reference scenario (**left**), a scenario without a MRS (**middle**) and the differences in bed level (**left - middle**) for the estuary channel (**right**)

4.3.5 Interplay

From the results of the subsystems it becomes evident that their interplay has large effect on the hydrodynamics and morphological development of the whole system. Opening a managed realignment site diverts a part of the estuary flow. The diversion increases the flow velocities from the downstream direction of the inlet towards the managed realignment site and slows the flow upstream of the inlet. The flood dominant flow direction is transferred onto the inlet, as the upstream side of the inlet erodes more (Figure 4.8). The flood dominant flow is transferred from the estuary through the inlet onto the basin, resulting in larger accretion rates in the top half of the basin. The other way around, the suction effect of the managed realignment site increase erosion downstream of the inlet, while deposition increase in the upstream direction.

The total volume change for the different subsystems can be found in Table 9. The system is importing cohesive sediment on a large scale, showing a positive volume change for the three different subsystems. Interestingly, only a very small volume of mud is able to settle in the inlet, indicating that the hydrodynamic activity remains high in this area. The inlet eroded severely, evident from the large loss of sand. The majority of the sediment eroded sediment is transported onto the basin. In addition, the total system is still able to import sand. The total system is accreting, where the majority of the import is cohesive sediment and change in sand volume is mostly a results of redistribution of local sediment.

Table 9: Summary of sediment volume changes for the three different subsystems after 25 years of morphological development.

Volume 1000m3	<i>sand</i>	<i>mud</i>	<i>total</i>
Basin	60.8	733.9	794.7
Inlet	-40.4	7.6	-32.8
Frontal inlet area	2.2	110	112.2
Total	22.6	851.5	874.1

4.4 Morphodynamic scenario modelling

The reference model is able to produce morphological development on the decadal scale that represents the infilling and evolution of a MRS. Morphodynamic scenario modelling is performed to understand how different forcings and design choices affect the long-term morphological development. This will help to understand the response of a MRS under different circumstances and make a generalisation for MRS projects in the future. The different scenario runs are repeated in Table 10 for convenience.

Table 10: description of morphodynamic scenarios. *Sediment concentration scenarios are ran with M2 tidal constituent only.

Scenario	Description
S1	
a	Reference scenario
b	Only ran with M2 tidal constituent
c*	SSC = 50mg/L
d*	SSC = 70mg/L
S2	
a	Inlet area based on the RCM (Townend, 2008)
b	Area increased to 2000x1400m

4.4.1 Inlet dynamics

The development of the inlet area below MSL for the different scenarios can be found in Table 11. Herein, a distinction is made between the inlet development in the first year and the final inlet area below MSL. The first year determines the how far from equilibrium the inlet is and the long-term development determines the equilibrium area below MSL.

The spring tidal prism of the managed realignment decreases in the absence of the S2 tidal constituent. The reduction in the maximum tidal prism consequently reduces the inlet area necessary to accommodate the flow through it, which is clearly visible from the reduction in inlet area below MSL of S1b after the 1st year of morphological development (Table 11). However, one would expect the final inlet area to remain significantly lower. This is not the case for two reasons. Firstly, the managed realignment site accretes less (Table 12), such that the maximum tidal prism relative to the beginning the inlet has to accommodate remain higher. Secondly, The inlet of scenario S1a is able to accrete a fraction of cohesive sediment above the critical mud content during neap tides (Figure 4.3). The increased shear stress for erosion of the cohesive sediment stabilizes the inlet. The lack of neap tides of S1B does not result in a sufficiently calm hydrodynamic period for cohesive sediment to reach the critical mud

content. Consequently, the critical shear stress for erosion is always governed by the more easily eroded non-cohesive sand fraction, increasing the inlet area. Increasing the suspended sediment concentrations (S1C & S1D) results in a smaller inlet area after the 1st year and after the full length of the morphological development. The increased presence of mud stabilizes the inlet and reduces the tidal prism by increased accretion (Table 12), showing the expected behaviour.

Table 11: Development of the inlet area below MSL for the morphodynamic scenarios.

scenario	Inlet area below MSL (m ²)		
	<i>initial</i>	<i>1st year</i>	<i>final</i>
S1			
a	252	521	480
b	252	480	472
c	252	475	429
d	252	468	397
S2			
a	582	654	568
b	426	768	908

Scenario S2a is on the only inlet that reduces in size over the full length of the morphological development, after a relatively small increase in inlet area after the first year. The stable inlet area is a product of the stable shape of the inlet over the course of the model run (Figure 4.18a). The channel only slightly adapts to the flood dominant direction of the flow. The regime channel method is thus able to predict a stable inlet area, preventing scouring and sand redistribution as opposed to a below equilibrium initial inlet area. Note that the shape of the regime channel consists of a single parabolic shape in contrast to the superposition of shapes as presented in Figure 2.6. Due to the flat initial basin, a sudden steep increase in surface area for a given tidal stage is present that dominates formation of the channel. The Large basin inlet grows significantly in the first year and keep growing after, while the basin continuous to accrete (Table 12), which is not expected. The increased width of the basin requires a larger drainage capacity, facilitated by the formation of channels just behind the dike. The channels erode the side of the inlet, widening it. This effect is more pronounced in the downstream direction, as the flood dominant flow is directed away from this location. The ebb dominant flow in the downstream section of the inlet continuous to scour and deepen (Figure 4.18b).

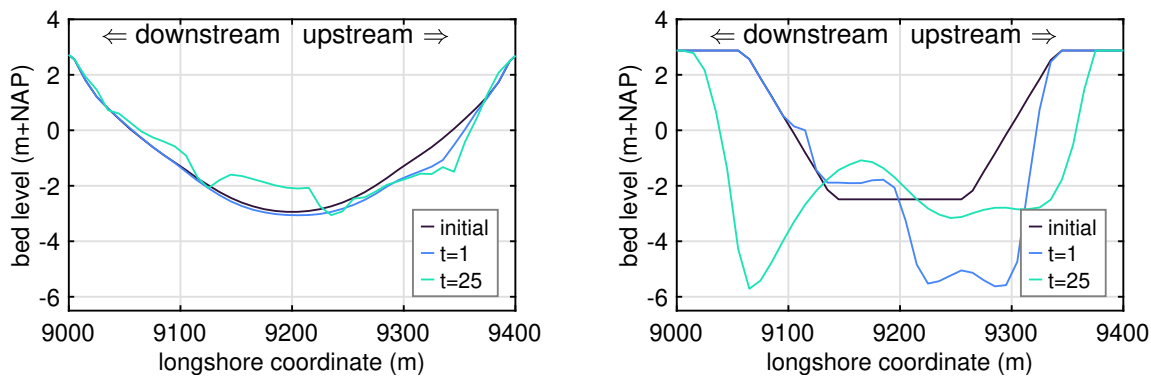


Figure 4.18: Inlet evolution for the managed realignment design scenarios. **left:** S2a and **right:** S2b.

4.4.2 Basin dynamics

The final accretion rates can be found in Table 12. Interestingly, a significantly smaller tidal amplitude does not lead to a strong reduction in the sedimentation. This is an effect of the increased trapping efficiency of mud. The diminished hydrodynamic activity transports less sediment onto the MRS during flood. During ebb a the diminished hydrodynamic activity resuspends less material and increases trapping efficiency.

As expected, a larger availability of suspended sediments results in a larger accretion of mud (scenario S1b - S1d Table 12). The increased amount of mud transport hampers the transport of sand. This becomes clear from the trapping efficiency of sand. A higher trapping efficiency of sand means that a larger proportion of sand transported onto the MRS remains, while the total accretion of sand is lower. The trapping efficiency of mud also increases for a higher sediment concentration. For low concentrations, a large parts may deposit close to the inlet, where hydrodynamic activity is high and erosion of the same sediments occurs during ebb. For higher SSCs a larger part of the mud is able to reach the back of the MRS, where hydrodynamic activity is limited, impeding resuspension of mud.

Table 12: Accretion rates and trapping efficiency for the different morphodynamic scenarios after 25 years of morphological development.

scenario	Accretion (cm)			Trapping efficiency (-)	
	<i>sand</i>	<i>mud</i>	<i>tot</i>	<i>sand</i>	<i>mud</i>
S1					
a-ref	4.2	50.6	54.8	0.44	0.53
b	3.7	47.0	50.7	0.41	0.55
c	3.1	62.5	65.5	0.42	0.57
d	3.0	77.0	80.1	0.48	0.57
S2					
a	0.7	53.1	53.8	0.32	0.56
b	4.1	54.5	58.5	0.18	0.57

Adapting the initial inlet area based on the RCM almost depletes the entire import of sand. The strong reduction in sand accretion is mostly caused by the absence of sand redistribution from the inlet. In term, the accretion of mud increases in absolute value and trapping efficiency. Adapting the MRS to local hydrodynamic and morphodynamic forcings is beneficial for the import of cohesive sediment, mostly found on intertidal wetlands. For a larger basin the import of both sediment fractions increases. After flood the distance from the mouth of the inlet to point furthest away increases. Therefore the slack period after flood increased, increasing the time for mud to deposit. As the non-cohesive sediment fraction is mostly dominated by bed load transport this effect does not occur. Sand is transporte in and out of the basin, but only a small part remains there, visible from the low trapping efficiency.

4.4.3 Estuary dynamics

The opening of a managed realignment side has an impact on estuary hydrodynamics and morphological development. From Figure 4.17 it became clear that the opening of a MRS caused sedimentation in the upstream direction of inlet and erosion in the downstream direction. The magnitude of the impact for the different scenarios is compared to assess whether these impacts are under the influence of local physical forcings and can be diminished by design choices.

herein, the accretion at the estuary side of the inlet and the estuary channel morphology are of importance.

The scenarios with increased suspended sediment concentrations are evaluated separately (Figure 4.19). The erosion and deposition pattern is not as clearly visible as is in the reference scenario (4.17). Deposition occurs along the entire length of the model (Figure 4.19a). However, The accretion of sediments is lower in the downstream direction of the inlet and higher in the upstream direction, in line with the reference scenario. This is most visible from the increased accretion to the intertidal wetland, indicating that suspended sediment downstream of the inlet are transported elsewhere. For larger suspended sediment concentration accretion in front of the inlet and on the intertidal wetland upstream of the MRS inlet increases, emphasizing the effect of the MRS.

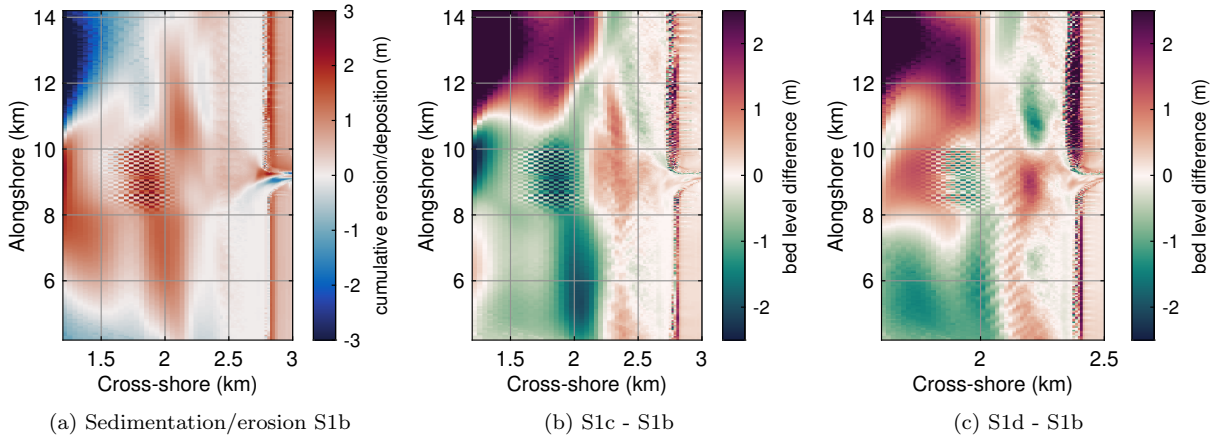


Figure 4.19: Cumulative erosion and deposition of S1b and the difference in final bed level. Positive values indicate an increase in deposition w.r.t. S1b.

The increased sedimentation in the upstream direction of the MRS and the extreme sedimentation at the western boundary are visible from the cumulative erosion and deposition of the reference scenario (Figure 4.20a). A smaller tidal range results in diminished hydrodynamic activity. The diminished hydrodynamic activity results in less severe sediment transport. As a result, areas of deposition in the reference scenarios show a negative bed level difference and vice versa compared to S1b (Figure 4.20b).

Next the effect of design choices is assessed. When the MRS is opened with an inlet closer to equilibrium, the initial channel is deeper and wider. The channel is fitted into the bathymetry, such that the channel extends to the point where the maximum depth of the channel and the alongshore depth of the estuary bathymetry are equal. The initial channels thus reaches further into the estuary, which has several effects. The wider and deeper channel remains wider and deeper limiting the sharp incision caused by the initial channel with an area below equilibrium (Figure 4.8). The wider inlet channel decreases the mean flow velocity in the direction of the channel, limiting the additional transport to the MRS. This is clearly visible from the general decrease in bed level in the estuary (Figure 4.20). However, there is region of increased erosion in front of the inlet. The MRS channel deposits sediment at the end of its inlet in the direction of the estuary, as the inlet channel of S2a reached further into the estuary, the deposition of this sediment is also directed more towards the estuary. When the basin area is doubled the tidal prism entering the MRS also doubled. The increased hydrodynamic activity amplifies the erosion and deposition patterns with respect to the reference scenario. This becomes clear when comparing Figure 4.19a with d. Areas of deposition show a positive bed level difference and

areas of erosion show a negative bed level difference. Enlarging the basin area thus amplifies the effect of the MRS, but does not alter its pattern.

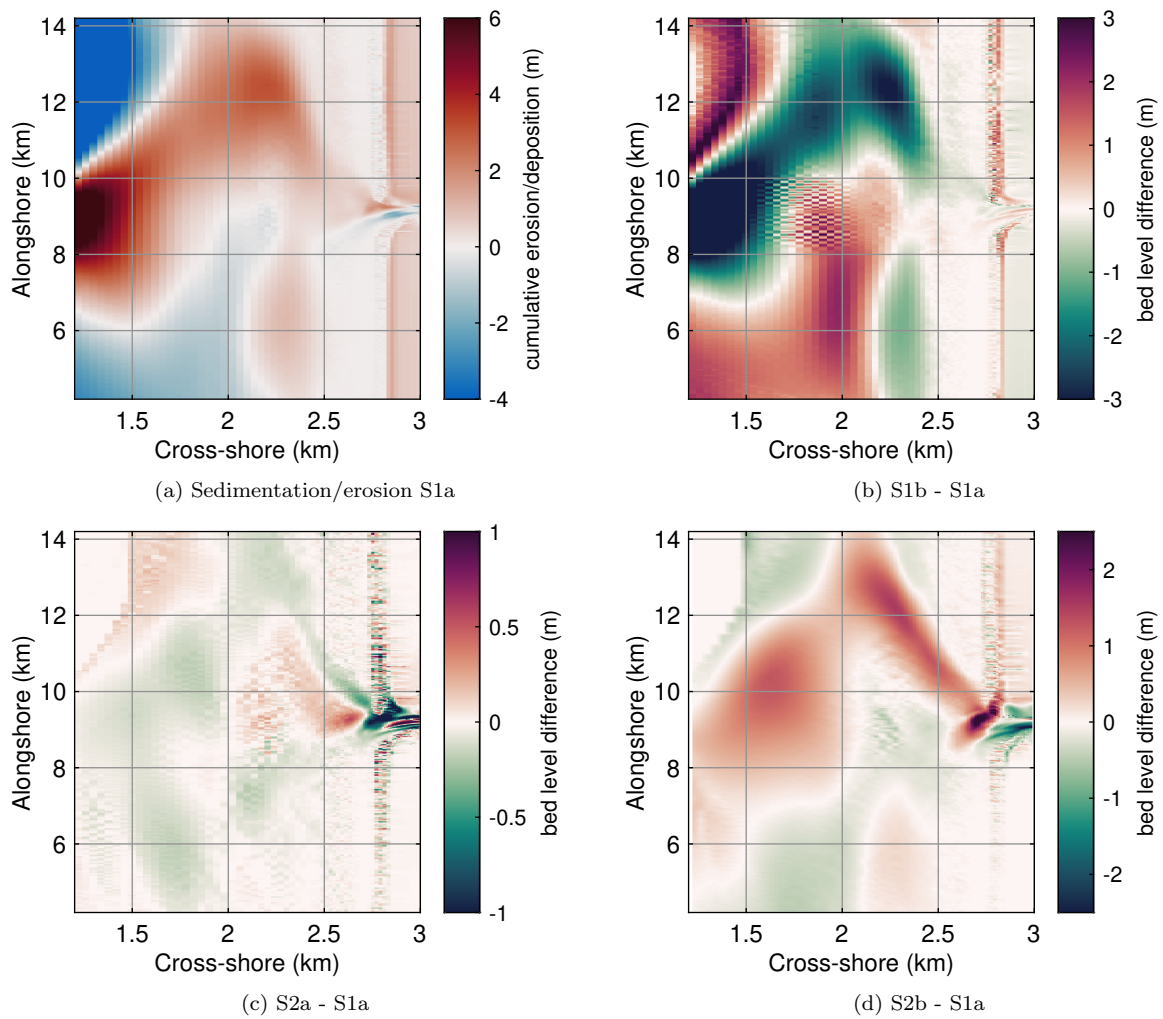


Figure 4.20: Cumulative erosion and deposition of S1a and the difference in final bed level. Positive values indicate an increase in deposition w.r.t. S1a. Note the different scales of the bed level differences for different scenarios

5 Discussion

This master thesis reports on the influence of different physical forcings and design choices on long-term morphological development of the managed realignment site, its inlet and its influence on the estuary channel. This section provides a discussion on the results of this study.

5.1 Reflection on the model and method

In this section, the consequences of the methodology that is used are discussed and a reflection is done on the implication for the results. It should be noted that S1b displays a checkerboard pattern in the middle of the estuary channel, which is normally the results of spurious oscillations in 3D simulations (Deltares, 2022a), as opposed to the 2DH simulation performed in this study. The sediment characteristic simulation were computed with the M2 tide only. Due to model limitations and time availability the scenarios could not be rerun.

5.1.1 Hydrodynamic boundary conditions

The hydrodynamic boundary conditions based on the Neumann water level gradients as produced by the combination of the M2 & S2 tidal constituents (Appendix A.5) is calculated for a characteristic water depth. The water depth is based on the initial maximum depth (-16m+NAP) plus MWL (0.18m+NAP) resulting in $H=16.18\text{m}$. As the morphology of the model develops the characteristic water depth changes and in term the values produced by the hydrodynamic boundary conditions. Over the 25 years of morphological development the bed lowers to -20m+NAP. Adjusting the boundary conditions to the new characteristic water depth would increase the velocity of the tidal wave, lowering the phase difference between the cross-shore boundaries. A faster travelling tidal wave would further erode the estuary channel and would in term require adjustment of the boundary conditions. The results is a loop of estuary channel deepening and changing boundary conditions. A common way to prevent the hydrodynamic boundary conditions from becoming unrealistic is by prescribing a constant bed level in the estuary channel (van der Wegen et al., 2017). This is partly achieved by the addition of a non-erodible layer in the model at a depth of -20m+NAP. This limits the change in the boundary conditions and disrupts the loop.

However, over the 25 years of morphological development a large amount of sedimentat deposits along the western boundary of the model (Figure 4.17). This is mostly caused by the addition of a third boundary point along the Western boundary in the middle of the estuary channel. The amplitude of the flow velocity is slightly increased (Figure C.1, increasing the sediment transport and consequently creating a artificial sedimentation pattern. The model is still able to produce the motion of the tidal wave over the full length of the simulation. Removing the extra boundary point or adding more boundary points along the western border may resolve the issue.

5.1.2 Morphological development

The morphological development is governed by the sediment transport routine of two sediment fractions that influence each other as explained in Appendix A.2. Herein, the critical shear stress for erosion is a governing model parameter for the sediment transport of cohesive sediment. It is a user-defined fixed value for which a cohesive sediment fraction erodes. The value of the critical shear stress for erosion ($\tau_{cr,m}=0.5\text{N/m}^2$) is based on on previous modelling studies into salt marshes in the Western Scheldt (Best et al., 2018; de Wilde, 2022; Willemsen et al., 2018). However, The value is relatively high compared to values found for weakly consolidated mud (van

Rijn, 2007a, $\tau_{cr,m}=0.2\text{N/m}^2$) and other modelling studies which focus more broadly on estuary development (Braat et al., 2017; van Kessel et al., 2011; Weisscher et al., 2022). In reality, the critical shear stress for erosion is under the influence of consolidation. As the cohesive sediment consolidates, the critical shear stress for erosion increases (van Rijn, 2007a) and becomes less prone to erosion. The high critical shear stress for erosion decreases the possibility for mud to resuspend and travel further up the basin. The chance for mud to travel further up the basin decreases and the bed stabilizes quickly. As the bed stabilizes, the location of morphological features (e.g. channels, sediment humps) within the MRS does hardly change (Figure 4.13). The in reality dynamic nature of the managed realignment site decreases as a result.

Additionally, consolidation lowers the soil with a typical value of 2mm/year for polders in the Western Scheldt (van Belzen et al., 2021). This value is probably higher in a recently restored intertidal area as there is a large amount of non-consolidated cohesive material imported. The newly imported sediment is in the primary consolidation phase (10-50 days) which is more rapid than the second phase (van Rijn et al., 2019), in which older sediment of a typical Western Scheldt polder is situated.

5.1.3 Model components

Initial bed composition

The initial bed composition consists of a single sediment fraction in the form of sand with $D_{50} = 200\mu\text{m}$. In reality the initial bed composition is a heterogeneous mix of a wide variety of sediments. The small intertidal wetland fronting the MRS generally consists of fine cohesive sediments (Willemsen et al., 2018) and sand fractions with a lower median grain size are found in the Perkpolder MRS (de Wilde, 2022). Additionally, the area behind the old dike consists of a mixture of light and medium clay (TNO, 2019), well consolidated due to prior use and the a dike typically consists of a sandy core with a clay layer on top. Already present fronting wetland consisting of cohesive sediments in the Western Scheldt are able to erode after opening of a MRS and the sediment is transported onto the MRS (de Wilde, 2022), in contrast to parts of the frontal wetland that are accreting in the model. However, well consolidated sediments due to prior agricultural use (increasing the shear stress for erosion) may lead to less a natural development of a MRS (Lawrence et al., 2018). The results have shown that initial configuration affect the long-term development of a MRS, emphasizing the influence the initial sediment composition can have on morphological development.

Waves

Waves are absent from the model and the scenarios presented in the sensitivity analysis due to numerical problems that arose in earlier version of Delft3D-FM. However, waves play a vital role in intertidal wetland and salt marsh dynamics. The salt marsh edge is affected by the daily long-term wave climate (Mariotti, 2020; Willemsen et al., 2018), as the lateral wave energy erodes the marsh edge (Kalra et al., 2021). However, wave edge erosion does not always lead to salt marsh loss when it is able to transgress landward (Kirwan et al., 2016) and eroded sediment can supply vertical accretion (Hopkinson et al., 2018). However, remnants of the old dike can acts as wave breakers (Hofstede, 2019), reducing the effect they have on the inner MRS. In addition, the basin is not sufficiently large for wind waves to form within the MRS, which can cause basin emptying without ample allochthonous sediment supply (Mariotti et al., 2017).

However, waves can still have significant effects on the morphological development of the MRS, as MRS under the influence of waves have a wider inlet area (Townend, 2008). Waves can erode the fronting wetland, resuspending sediment able to vertically accrete the MRS. Waves reaching the inlet would have significant impact in two ways. First, enhanced bed shear stress

by wave activity would lower the residual capacity before the critical bed shear stress for erosion is exceeded. As a result, the inlet would need to be bigger to accommodate a given discharge. Second, Waves reaching the inlet of the MRS would brake, eroding the the remaining sea wall widening the inlet area (Townend, 2008). In theory, a wider inlet is less efficient and flow velocities in the inlet reduce, lowering possible transport onto the MRS and increase inlet deposition. The effect of waves remains to be seen, but can be significant.

Vegetation

Part of a managed realignment site is the reintroduction of salt marsh vegetation and its potential effects on hydrodynamics and morphology. The effects of vegetation are excluded from the model as the initial elevation is low and vegetation only develops above a certain elevation threshold (Balke et al., 2016). In addition, an inundation-free period is required for initial establishment, followed by a relatively calm period with low waves and limited bed level dynamics for subsequent growth (Hu et al., 2015; Poppema et al., 2019). Nevertheless, the start of vegetation typically starts after approximately 25 years (van Belzen et al., 2021) and its effects can have a significant impact long-term development and are discussed.

Vegetation slows down the flow due to increased drag and stabilizes the soil, increases the trapping efficiency of sediments (Friess et al., 2012), in term increasing the accretion rates of the the MRS. In addition, the accumulation of biomass due to vegetation growth can increase accretion (Morris et al., 2002). The areas with maximum elevation near the inlet (Figure 4.13) suggests that vegetation is most likely to establish in that region. Consequently, the soil around these patches stabilize, continue to accrete and accumulate biomass. In addition, the increased drag might hinder sediment transport onto the landward end of the basin. The formation of high elevated areas near the inlet may create unfavorable circumstances for infilling of the MRS over the long-term.

5.1.4 Conclusion of static model

The main morphological trends are captured by the model. A reduction in hydroperiod reduces the accretion rates (Morris, 2012; van Belzen et al., 2021), the inlet grows as its area is below equilibrium (Townend, 2008) and a network of channels forms as present in a typical managed realignment site. However, the combination of processes that are excluded from the model make it static, as opposed to the highly dynamic intertidal and complex system it in reality is.

5.2 Model as part of a larger system

The model domain consists of a straight estuary channel, without spatial variability in the along-shore direction. The tidal motion and corresponding flow velocities are reproduced properly. However, the effects of hydrodynamic and morphological estuary features such as a funneling shape, bed slope, river discharge and secondary flow are excluded from the model results. Ladd et al. (2021) stresses the importance of estuary wide morphological development of intertidal wetlands and the effect of the position of the wetland with respect to the estuary channel. Although flow velocities are reproduced fairly well, the peak flow velocities are lower than in the Western Scheldt, in line width Leuven et al. (2018), where the more complex shape of the Western Scheldt produces higher peak flow velocities then based on the regression analysis (Figure 4.1).

Only part of the estuary channel is modelled, resulting in a water level boundary that bisects the channel. Over the entire length of the simulation a huge amount of sediment accumulates near

the boundary (Figure 4.17). As a result, the model is only capable of predicting the influence of the MRS on the near inlet morphology.

To diminish the effect of the boundaries they should be placed sufficiently far away from the area of interest. As such, increasing the size of the model domain would be beneficial for the results. An estimate of the distance between the boundary and the area of interest can be made by the length the flow travels during half a tidal cycle. As such, the flow through the boundaries is not able to reach the area of interest. The mean flow velocity during a flood spring tide is 0.96m/s. Multiplying with the duration of half a tidal cycle of 6 hours results in boundaries that would need to be over 20.6km away from the area of interest. The alongshore domain would increase from 14km to over 41.6km. Simulating the entire width of for example the Western Scheldt at the Hellegatpolder would increase the cross-shore domain from 2km to 4.5km. The domain would increase 6 fold, significantly increasing the already vast computational time and lies beyond the scope of this research.

Capturing the effects breaching part of a dike to create a managed realignment site is of great importance. Opening a managed realignment site does not necessarily lead to an increase in flood safety. A new subsystem is created as the tidal flow is largely separated from the main estuarine water body. The tidal prism increases, without any compensatory increase in the cross-sectional area of the estuarine channel. The estuary is forced to increase its cross-sectional area by erosion to accommodate the increased tidal flow demanded by the restored site. In doing so, existing intertidal wetlands areas in the rest of the estuary may erode (Pethick, 2002; Townend et al., 2002). This is supported by findings from Weisscher et al. (2022) who found that opening a MRS leads to an increase in tidal prism along the entire estuary in most cases and an increase in water level in some location based on the location, width of the inlet and number of polders opened. In addition, when planning subsequent projects, the order in which these projects are carried out influences the hydromorphological development of the area itself, but also influences the hydrodynamics of the larger system (Weisscher et al., 2022). Lastly, modelling the managed realignment site as part of a larger system can give insight into the sediment budget of a system. Assessing the sediment budget for an entire system is key for determining the development and more important the survival of intertidal wetlands (Ganju, 2019).

5.3 Inlet development

Correctly predicting inlet dimensions and development is important as it can have an impact on the hydromorphological development of a MRS (Friess et al., 2014; Townend et al., 2010). A conventional way of calculating the equilibrium inlet dimensions is by means of an A-P relationship. The problem with such relationships is their inability to incorporate physical information about the system and as such they can only be used for systems with phenomenological similar characteristics (Stive et al., 2011). The equilibrium inlet area below MSL based on the tidal prism of the model is calculated for several of these relationships as present in literature (Figure 4.4). None of the relationships are able to correctly predict the inlet area based on the tidal prism from the model. The A-P relationship from Hume (1991, no causeways) is based on inland estuaries (thus sheltered from waves), comparable tidal prism and similar sediment characteristics (fine sand and a proportion of mud), and shows the best comparison with the inlet area as produced by the model. However, the relationships still severely underestimate the inlet area, especially for smaller tidal prisms. A possible explanation is the difference in bathymetry. The estuaries start at a larger depth and tidal exchange occurs during the entire tidal cycle. The tidal basin remains dry for extended periods of time, as its elevation is situated above low tidal water levels, limiting tidal exchange during part of the tidal cycle. A comparable

tidal prism thus has to pass through the inlet in less time, increasing the flow velocity, erosion and the inlet area.

Literature with a focus on determining empirical coefficients for A-P relationships tend to categorize inlets based on a range of classes (e.g. Table 4). For example Jarrett (1976) already presents 15 different combinations of empirical coefficients and one can always relate a certain combination by trial and error, while system characteristics do not comply. As such, it is argued that although the inlet may comply with a single variation, this does not necessarily hold for other managed realignment sites or even the same managed realignment site with a different initial design.

The more physical based analytical approach (Townend, 2008), allows inclusion of information about MRS conditions. The regime channel method was able to produce bounds, based on sediment characteristics, wherein the area below MSL is always situated for a case study of a MRS in the Western Scheldt (Figure 3.2) and based on idealized model results (Figure 4.4). Herein, it took several years for the inlet area of the case study to adapt to the highly dynamic initial situation. Additionally, the RCM produces inlet dimensions and shape for the full range of tidal datums as opposed to A-P relationships, where the shape of the channel can significantly influence its dimensions (Hume, 1991; Townend, 2008). As such, the RCM could be used as a starting points to determine inlet dimensions of a MRS in the Western scheldt.

Results of the regime channel method should be taken with care. Attention should be given to the sediment characteristics, as the outcome of the RCM is heavily dependant on the critical shear stress of the present sediment fractions. For the Perkpolder detailed sediment characteristics were available. In case of the model, the regime channel method complies to the user-defined input of the sediment fractions. However both fractions have been altered according to Eq. A.2 under the presence of mud. Not altering the critical shear stress of sand would result in a wider range of values wherein the area below MSL can be situated. For example, when the critical shear stress for erosion of sand is not altered, the bounding interval after 20 years of morphological development wherein the inlet area below MSL lies increases from 136m² to 414m². Uncertainty in sediment characteristics thus lead to a significant growth of the bounding interval.

Secondly, Many recently opened managed realignment sites are breached with an inlet area far below their equilibrium (de Wilde, 2022; Friess et al., 2014; Hume, 1991; Pontee et al., 2019). After opening, the same tidal prism has to pas trough a small inlet area, increasing flow velocities. As a results, bed scouring creates a relatively deep channel width a lower width/depth ratio (Hume, 1991) then produced by the RCM. The deeper channel is more efficient and the minimum bed level in the inlet can be below the minimum bed level that can be produced by the RCM. This behaviour is present from the reference scenario as well as from real world cases. When the MRS is opened with sufficient inlet area below MSL, the minimum bed level in the inlet is the same as the minimum bed level as predicted by the RCM (Figure 4.18a). The RCM method is always a symmetrical superposition of parabolic shapes and not able to capture the influence of the dominant flow direction on inlet shape.

Model results agree with findings from Friess et al. (2014) and Townend et al. (2010). The initial sediment 'humps' caused by the redistribution of below equilibrium inlet sand continue to influence the morphodynamic development of the basin in the long-term. Model results have also shown that an initial inlet are below MSL closer to equilibrium favors the import of cohesive sediment onto the MRS (Table 12). These results emphasize the importance of initial inlet shape and dimensions on long-term morphological development. Similar humps can also be seen in the Perkpolder MRS at the end of the pond (figure 3.1), although its effect on long-term morphodynamic behaviour is not yet known.

Part of the RCM is based on an empirical formula to determine the depth and parabolic shape. The empirical coefficients are based on salt marsh channels in the UK. These salt marshes have comparable tidal ranges in some cases. Determining the empirical coefficients based on salt marshes in the Netherlands (especially in the Western Scheldt) may lead to better results, but is beyond the scope of this research.

Lastly, the effect of friction and waves are not taken into account by the RCM. These can be included as further explained in Townend (2008). The waves were not incorporated due to priorly present model limitations. The friction can be incorporated as a phase lag in the vertical rate of the water surface within the site, but by means of the small basin principle (Bosboom et al., 2021), the differences in water level between estuary and the MRS are negligible.

Sharp channel incision was present in the inlet of scenario S2b (Figure 4.18). It is suspected that this is a result of the low value of the user-defined value for the transverse bed load transport (Appendix A.4). The flow seems to prefer flowing through as few grid cells as possible (Baar et al., 2019). The relatively small grid cell size causes channel incision. The user-defined value for the transverse bed slope is insufficient to overcome the channel incision.

5.4 Accretion rates and patterns

Accretion rates of the model are in line with accretion rates from managed realignment sites with similar hydrodynamic characteristics (Table 7). The accretion rates diminish over time as the bed level rises and consequently the hydroperiod is reduced, in line with the general trend for managed realignment sites (Morris, 2012). The accretion pattern is twofold. Part of the suspended sediment is transported onto the back of the basin creating a landward to seaward infilling and a large sediment accretion is found near the inlet between the main channels. The landward to seaward infilling is typical for managed realignment sites as can be seen from field observations (Lawrence et al., 2018) and models (Gourgue et al., 2022). However, seaward to landward infilling is less common. A possible explanation is the position in the tidal frame. This allowed the transportation of sand onto the basin during the first few years of morphological development (Figure 4.12). This is in line with field observations from the Perkpolder, where a deep pond is filled with relatively coarse sediments and fine sediments are transported onto the back of the basin (de Wilde, 2022) and model results from opening a managed realignment site in the Western Scheldt at the same location as the model presented here (Weisscher et al., 2022).

The effect of opening a MRS on the estuary can be clearly seen from Figure 4.17. The erosion and deposition patterns are in line with those of Weisscher et al. (2022). The additional flow from the downstream direction of the inlet erodes the estuary and deposition increases in the upstream direction of the inlet. However, the magnitude of estuary erosion and deposition as presented by Weisscher et al. (2022) is three times as large compared to the results presented here. The most likely explanation is the difference in hydrodynamics and bathymetry. The estuary channel is deeper in the model presented by (Weisscher et al., 2022), increasing the flow velocities and thus erosion. Furthermore, the more complex bathymetry can also increase the flow velocities (i.e. the funnelling shape). The effect of the increased erosion deepens the channel further creating a knock on effect and consequently the differences in magnitude.

Comparing the model with a recently opened managed Perkpolder managed realignment site reveals some interesting differences. Although the accretion rates are comparable, the location of the accretion differs vastly. Accretion in the Perkpolder is most pronounced in the pre-dug channels (Figure 5.1), comparable with the sedimentation of the pre-dug channel of the model. However, the magnitude of landward to seaward infilling as produced by the model is not seen



Figure 5.1: Bed level difference between 2016 & 2022 in the intertidal area of Perkpolder managed realignment site. North of bed level differences lies the deep pond.

in the Perkpolder. Accretion on the intertidal area of the Perkpolder is very limited, which is caused by a combination of reasons. The intertidal area mostly accretes fine sediments (van de Lageweg et al., 2019). These fine sediments tend to consolidate significantly more (van Rijn et al., 2019) than the sandy sediments deposited in the channels. The consolidation of sediment causes the bed level to lower due to settlement. This process is not included in the model, increasing the accretion rates at the landward.

The Perkpolder also shows significant sedimentation at the beginning of the intertidal area south of the pond. this is in line with formation of the sediment humps around the main channel (Figure 4.11). However, the magnitude of sedimentation and the maximum elevation are higher in the model due to three reasons. Firstly, the cohesive sediments that deposit do not consolidate. Secondly, the deposited cohesive sediment shelter the more easily erodible sand layer as a result of high initial inlet redistribution of sediments. Thirdly, it is suspected that the user-defined parameter governing the transverse bed load transport bed load transport is governed by a user-defined parameter (Appendix A.4) is to low. As a result, the magnitude of down slope bed load sediment transport is low and the humps of sediment retain their high elevation.

6 Conclusion

The aim of this research to determine hydromorphological interplay between the estuary, the inlet and the managed realignment site as a result of dike breaching and subsequent reintroduction of tidal exchange.

1. What are the driving factors for breach evolution after opening managed realignment site?

Model results show that the conventional empirical relationships are unable to correctly predict the equilibrium inlet area below MSL of a managed realignment site. The regime channel method based on the Perkpolder data and model results produced bounds based on two representative sediment fractions. It was able to correctly predict the inlet dimensions below MSL in the Perkpolder after it adapted to the high dynamic initial situation. Inlet development by the model also complied to the bounds as created by the regime channel method after adaptation to the high dynamic initial situation. The inlet area below MSL stayed within this bounds throughout the examined time period for both cases. The regime channel method is unable to correctly predict the effect of the dominant flow direction on inlet evolution. The use of the regime channel method revealed three driving factors.

1. The hydrodynamics are governed by the spring tidal prism. The spring tidal prism determines the surface area, water level and vertical velocity for different tidal stages. The regime channel is calculated for every tidal stage. The resultant channel is the superposition of the regime channels.
2. The hypsometry of the basin is essential to produce a superposition of regime channels that produce the final shape. A lack of vertical spatial variety in the managed realignment sites produces a single parabolic shape. After opening the natural development of the managed realignment site will produce vertical spatial variety and the single parabolic shape will not hold.
3. The regime channel method inlet dimensions below MSL produces bounds based on site sediment characteristics. Altering these characteristics can alter the bounds significantly. Results shown that the best estimation was produced by using a sand sediment fraction under the influence of stabilizing cohesive sediment.

2. How does a managed realignment site in an estuarine environment develop on the decadal scale?

After opening, the development of the managed realignment site is governed by the adaptation of the inlet to local hydrodynamics and sediment characteristics. This becomes evident from the large increase in inlet area below MSL for both the Perkpolder and model results. The majority of the sediment from the inlet and from the frontal inlet area is transported onto the MRS acting as a sediment source.

Initially the accretion rates in the managed realignment site are very high due to two reasons. First, the initial redistribution of inlet sand is transported onto the managed realignment site, while the transport of sand quickly reduces after the first year. Secondly, a longer hydroperiod increases the time for cohesive sediment to settle. As the elevation in the basin rises, the hydroperiod reduces and the accretion rates reduce as a results.

within the basin, the redistribution of sediments initiates the formation of channels. Herein, the broad and shallow pre-dug channel deepens and narrows. The main channels branch out

in the landward direction splitting into smaller channels. The formation of channels promotes flow onto the back of the basin. Parallel, the formation of sediments 'humps' in between the channel start to form creating high elevated area close to the inlet.

Over the long-term a network of channels is created. During this period there are two distinct sedimentation patterns. The first is the typical landward to inlet infilling of cohesive sediment that are able to transport with the flow and settle where hydrodynamic activity is lowest. The second is the formation of high elevated areas near the inlet between the main channel branches. This is partly an artifact of the initial redistribution of sand, but these areas persist to accrete over the long-term, indicating the importance of initial design on the long-term development of a managed realignment site.

3. What is the influence of physical forcings on the hydrodynamic and morphological development of a managed realignment site?

A reduction in the tidal amplitude reduces the transport of suspended sediment onto the managed realignment site. As a result the total accretion lowers 4.1cm over a 25 year span. The reduction in hydrodynamic activity increases the trapping efficiency, as during ebb flow conditions previously settled cohesive sediment is less easily re-eroded. Due to the absence of the spring-neap effect mud is not able to settle in the inlet during calm neap tides. In combination with the diminished accretion and consequently larger tidal prism the inlet area remains relatively large compared to the combination of an M2 and S2 tidal constituent. The reduced hydrodynamic activity in the estuary reduces the magnitude of the erosion and deposition.

A higher sediment suspended sediment concentration leads to a higher accretion rate. As mud becomes more abundant the transport of sand is reduced. As mud accretes it shelters the more easily eroded sand, increasing the trapping efficiency for larger suspended sediment concentrations for both sand and mud. The increased accretion lowers the hydroperiod, reducing the time for sediment to settle, but at the same time reduce erosion during ebb flow conditions. The decrease in tidal prism allow cohesive sediments to settle in the inlet, stabilizing it and lowering the inlet area below MSL. The effect of the managed realignment site on estuary erosion and deposition become more pronounced.

4. What is the influence of managed realignment site design choices on the hydrodynamic and morphological development of a managed realignment site?

Starting with an inlet area closer to equilibrium increases the accretion of cohesive sediments and the trapping efficiency. in term, the initial redistribution of sandy sediment from the inlet is reduced severely, consequently reducing the accretion of sand in the basin. Interestingly, the initial dimensions and shape of the inlet as produced by the regime channel method only changes slightly over the full length of the morphological development. In term, the effect of the MRS on estuary erosion and deposition is diminished. Increasing the basin area increases the tidal prism and in term the sediment transport onto the managed realignment site. The increased sediment transport is visible from the increased accretion rate and trapping efficiency. Consequently, a larger division of the tidal flow increases the effect of the MRS on estuary erosion and deposition.

7 Recommendations

In this thesis, the focus lies on the long-term morphological development of a managed realignment site under the influence of different physical forcings and design implementations. This section provides recommendations to improve the predictions of long-term morphological development and provide more effective design standards for future realignment projects.

7.1 Insight for managed realignment projects

From a Nature-Based Solutions perspective, disturbances should be kept to a minimum. The opening of the managed realignment site is a disturbance in itself and proper design for the long-term objective is importance to minimise additional disturbances. This section proposes improvements for the design of future managed realignment projects.

Inlet adaptation

The adaptation of the inlet area to an equilibrium situation has been investigated. The results have shown that the regime channel method is able to predict the inlet area below MSL for a case study and with a numerical model. An initial design with an inlet area closer to equilibrium is able to import a larger amount of cohesive sediment onto the managed realignment site, as well as reduce its impact of the estuary bathymetry. The initial inlet area should be considered in the design of future managed realignment sites to maximize its potential and minimize disturbances.

The change in inlet morphology to an equilibrium situation is the largest during the first few years after opening a managed realignment site. The use of the regime channel method has shown that the sediment characteristics determine the bounds wherein the equilibrium inlet area is situated. A measurement campaign should be conducted prior to opening to determine these characteristics. The regime channel method can then be combined with more detailed simulation to determine the inlet area after opening

Natural development

The goal of a managed realignment project is to recreate a formerly present intertidal wetland. Well consolidated material due to former agricultural use leads to less natural development (Lawrence et al., 2018). This thesis has shown that the high critical shear stress for erosion of cohesive sediment may limit the resuspension of sediment and hamper the natural development. Therefore, it may be beneficial to loosen the soil prior to opening a managed realignment site. This way, the natural redistribution of sediment and the self-organizing nature of intertidal wetland can be enhanced.

Influence on estuary morphology

Opening a managed realignment site influences the estuary morphological development. This research has shown that sedimentation occurs at the end of the pre-dug inlet channel on the estuary side, in line with observations from the Western Scheldt (de Wilde, 2022). However the magnitude is small and not in line with other modelling studies (Weisscher et al., 2022). The effects of the managed realignment site needs to be investigated further. Large amounts of deposition in the estuary channel can have large implications for anthropogenic use of the estuary such as shipping.

Further investigation into the effects of opening a managed realignment site on estuary hydrodynamics and morphological development is necessary. It is recommended to hindcast the the morphological development of the entire Western scheldt after opening of the Perkpolder up until the present day. From here, the same model can be used to assess the morphological

development of the Western Scheldt without opening of the Perkpolder. This the difference in model results provides a good indication of the effect of the opening of a managed realignment. The model can also be further extended to determine its effect on long-term morphology and the hydrodynamics.

7.2 Model improvements

The model produces fairly static results, while the opening of a managed realignment site has a high dynamic nature. To achieve a better representation of this dynamic behaviour improvements can be made to the morphological model.

Morphodynamics

The use of a single value for the critical shear stress for erosion of cohesive sediment provides a bad representation of reality. It is recommended to determine the influence of a more realistic sediment transport routine on the long-term development of a managed realignment site. An example of such a routine is the fluff layer concept as presented in van Kessel et al. (2011). Herein, the recently deposited sediment is able to resuspend more easily. This provides a more realistic description of cohesive sediment that are not yet consolidated and thus have a lower critical shear stress erosion.

The model showed large accretion rates at the landward end of the basin, contrarily to the accretion rates of the Perkpolder managed realignment site. The difference in accretion is the result of the lack of a consolidation routine within the module. Primary consolidation can increase the dry bulk density significantly over the first 50 days (van Rijn et al., 2019), lowering the bed and thus the accretion rate. In order to properly represent the long-term development of a managed realignment site a consolidation module is a necessity. An example of an efficient consolidation module suitable for long-term morphodynamic simulations efficient consolidation module suitable for long-term morphodynamic simulations for muddy systems is presented in Winterwerp et al. (2018)

Hydrodynamic

The hydrodynamic boundary conditions are forced by the use of combination of water levels and its gradients. The boundaries correctly reproduced the motion of the tidal wave propagating through the estuary. Its effect on inlet and basin morphology can be clearly seen from the results. Additionally, the effect of the dominant flow direction on inlet morphology becomes clear from the bed level development of the Perkpolder over the period between 2016 - 2022. It is recommended to include the effect of estuary hydrodynamics on the long-term development of a managed realignment site. However, further investigation about the use of the Neumann boundaries used in this study requires further investigation. Time and computational resources in this study are limited and increasing the model domain to such an extent that the boundaries don't influence the managed realignment site can have a large influence on the morphological development of the managed realignment site.

7.3 Additional scenarios

Most managed realignment sites are opened with a network of pre-dug channels, such as the Perkpolder and the Hedwiges-Prosperpolder. The effect of adding a variety of channels is not investigated. Channels increase the conveying capacity of the site, allowing the flow to reach the back of basin more easily. Increasing the conveying capacity may increase the typical landward to seaward infilling of the system. The effect on the long-term development

Results have shown that sedimentation is larger in the dominant flow direction of the estuary (flood in this case). As such, placing the inlet more downstream (so that a larger area of the

MRS is in the dominant flow direction with respect to the inlet) may improve accretion rates. Increasing the inlet area below MSL to a value above equilibrium and placing multiple smaller inlets can also be interesting scenarios. Placing multiple inlet can have a negative impact on estuary water levels (Pontee, 2015).

The influence of waves should be added. The effect of waves on the morphological development of natural salt marshes is widely known and a controlling factor in the long-term morphological development (Mariotti, 2020; Willemsen et al., 2018). Waves can also significantly impact inlet dimensions (Townend, 2008) and can have a large impact on managed realignment morphological development (de Wilde, 2022). The impact of waves on long-term development of a managed realignment site should be investigated and if significant taken into account for the initial design phase. Although, a managed realignment site such as the Perkpolder is mostly sheltered from the dominant wind direction, the effect of ship induced waves can have play a major part in the erosion of tidal flats (Schroevens et al., 2011).

References

- Ashworth, P. J., Best, J. L., & Parsons, D. R. (2015). *Fluvial-tidal sedimentology*. Elsevier.
- Baar, A., Boechat Albernaz, M., Van Dijk, W., & Kleinhans, M. (2019). Critical dependence of morphodynamic models of fluvial and tidal systems on empirical downslope sediment transport. *Nature communications*, *10*(1), 4903. <https://doi.org/10.1038/s41467-019-12753-x>
- Balke, T., Stock, M., Jensen, K., Bouma, T. J., & Kleyer, M. (2016). A global analysis of the seaward salt marsh extent: The importance of tidal range. *Water Resources Research*, *52*(5), 3775–3786.
- Best, Ü., Van der Wegen, M., Dijkstra, J., Willemsen, P., Borsje, B., & Roelvink, D. J. (2018). Do salt marshes survive sea level rise? modelling wave action, morphodynamics and vegetation dynamics. *Environmental Modelling & Software*, *109*, 152–166. <https://doi.org/https://doi.org/10.1016/j.envsoft.2018.08.004>
- Borsje, B. W., van Wesenbeeck, B. K., Dekker, F., Paalvast, P., Bouma, T. J., van Katwijk, M. M., & de Vries, M. B. (2011). How ecological engineering can serve in coastal protection. *Ecological Engineering*, *37*(2), 113–122. <https://doi.org/https://doi.org/10.1016/j.ecoleng.2010.11.027>
- Bosboom, J., & Stive, M. J. (2021). Coastal dynamics. <https://doi.org/https://doi.org/10.5074/T.2021.001>
- Braat, L., van Kessel, T., Leuven, J. R. F. W., & Kleinhans, M. G. (2017). Effects of mud supply on large-scale estuary morphology and development over centuries to millennia. *Earth Surface Dynamics*, *5*(4), 617–652. <https://doi.org/10.5194/esurf-5-617-2017>
- Bridges, T. S., King, J. K., Simm, J. D., Beck, M. W., Collins, G., Lodder, Q., & Mohan, R. K. (2021). International guidelines on natural and nature-based features for flood risk management.
- Brunetta, R., de Paiva, J. S., & Ciavola, P. (2019). Morphological evolution of an intertidal area following a set-back scheme: A case study from the perkpolder basin (netherlands). *Frontiers in Earth science*, *7*, 228.
- Byrne, R., Gammisch, R., & Thomas, G. (1980). Tidal prism-inlet area relations for small tidal inlets. In *Coastal engineering 1980* (pp. 2517–2533).
- Callaghan, D., Bouma, T., Klaassen, P., van der Wal, D., Stive, M., & Herman, P. (2010). Hydrodynamic forcing on salt-marsh development: Distinguishing the relative importance of waves and tidal flows. *Estuarine, Coastal and Shelf Science*, *89*(1), 73–88. <https://doi.org/https://doi.org/10.1016/j.ecss.2010.05.013>
- Cao, S., & Knight, D. W. (1997). Entropy-based design approach of threshold alluvial channels. *Journal of Hydraulic Research*, *35*(4), 505–524.
- Costanza, R., d’Arge, R., De Groot, R., Farber, S., Grasso, M., Hannon, B., Limburg, K., Naeem, S., O’neill, R. V., & Paruelo, J. (1997). The value of the world’s ecosystem services and natural capital. *nature*, *387*(6630), 253–260.
- Cousins, L., Cousins, M., Gardiner, T., & Underwood, G. (2017). Factors influencing the initial establishment of salt marsh vegetation on engineered sea wall terraces in south east england. *Ocean & Coastal Management*, *143*, 96–104.
- Dam, G. (2013). *Harde lagen westerschelde*.
- De Mesel, I., Ysebaert, T., & Kamermans, P. (2013). *Klimaatbestendige dijken: Het concept wisselpolders* (tech. rep.). IMARES.
- de Vriend, H. J., Wang, Z. B., Ysebaert, T., Herman, P. M. J., & Ding, P. (2011). Eco-morphological problems in the yangtze estuary and the western scheldt. *Wetlands*, *31*, 1033–1042. <https://doi.org/https://doi.org/10.1007/s13157-011-0239-7>

- Dean, R. G. (1991). Equilibrium beach profiles: Characteristics and applications. *Journal of coastal research*, 53–84.
- Deltares. (2022a). *Delft3d fm suite: D-flow manual*.
- Deltares. (2022b). *Delft3d fm suite: D-morphology manual*.
- de Wilde, T. (2022). Hydrodynamic and morphodynamic response of perkpolder after a managed realignment.
- Duarte, C. M., Dennison, W. C., Orth, R. J., & Carruthers, T. J. (2008). The charisma of coastal ecosystems: Addressing the imbalance. *Estuaries and coasts*, 31, 233–238.
- Dunn, F. E., Darby, S. E., Nicholls, R. J., Cohen, S., Zarfl, C., & Fekete, B. M. (2019). Projections of declining fluvial sediment delivery to major deltas worldwide in response to climate change and anthropogenic stress. *Environmental Research Letters*, 14(8), 084034.
- Duong, T. M., Ranasinghe, R., Luijendijk, A., Walstra, D., & Roelvink, D. (2017). Assessing climate change impacts on the stability of small tidal inlets: Part 1 - data poor environments. *Marine Geology*, 390, 331–346. <https://doi.org/https://doi.org/10.1016/j.margeo.2017.05.008>
- Esteves, L. S. (2014). Methods of implementation. In *Managed realignment : A viable long-term coastal management strategy?* (pp. 33–44). Springer Netherlands. https://doi.org/10.1007/978-94-017-9029-1_3
- Fagherazzi, S., Kirwan, M. L., Mudd, S. M., Guntenspergen, G. R., Temmerman, S., D’Alpaos, A., Van De Koppel, J., Rybczyk, J. M., Reyes, E., Craft, C., et al. (2012). Numerical models of salt marsh evolution: Ecological, geomorphic, and climatic factors. *Reviews of Geophysics*, 50(1).
- Friedrichs, C. (2011). Tidal flat morphodynamics: A synthesis. *Treatise on Estuarine and Coastal Science*, 3, 137–170.
- Friess, D. A., Krauss, K. W., Horstman, E. M., Balke, T., Bouma, T. J., Galli, D., & Webb, E. L. (2012). Are all intertidal wetlands naturally created equal? bottlenecks, thresholds and knowledge gaps to mangrove and saltmarsh ecosystems. *Biological Reviews*, 87(2), 346–366.
- Friess, D. A., Möller, I., Spencer, T., Smith, G. M., Thomson, A. G., & Hill, R. A. (2014). Coastal saltmarsh managed realignment drives rapid breach inlet and external creek evolution, freiston shore (uk). *Geomorphology*, 208, 22–33.
- Ganju, N. K. (2019). Marshes are the new beaches: Integrating sediment transport into restoration planning. *Estuaries and Coasts*, 42(4), 917–926.
- Gerwing, T. G., Davies, M. M., Clements, J., Flores, A.-M., Thomson, H. M., Nelson, K. R., Kushneryk, K., Brouard-John, E. K., Harvey, B., & Plate, E. (2020). Do you want to breach an embankment? synthesis of the literature and practical considerations for breaching of tidally influenced causeways and dikes. *Estuarine, Coastal and Shelf Science*, 245, 107024.
- Gourgue, O., van Belzen, J., Schwarz, C., Vandenbruwaene, W., Vanlede, J., Belliard, J.-P., Fagherazzi, S., Bouma, T. J., van de Koppel, J., & Temmerman, S. (2022). Biogeomorphic modeling to assess the resilience of tidal-marsh restoration to sea level rise and sediment supply. *Earth Surface Dynamics*, 10(3), 531–553.
- Hofstede, J. L. (2019). On the feasibility of managed retreat in the wadden sea of schleswig-holstein. *Journal of Coastal Conservation*, 23(6), 1069–1079.
- Hopkinson, C. S., Morris, J. T., Fagherazzi, S., Wollheim, W. M., & Raymond, P. A. (2018). Lateral marsh edge erosion as a source of sediments for vertical marsh accretion. *Journal of Geophysical Research: Biogeosciences*, 123(8), 2444–2465.

- Horstman, E. M., Dohmen-Janssen, C. M., Bouma, T. J., & Hulscher, S. J. (2015). Tidal-scale flow routing and sedimentation in mangrove forests: Combining field data and numerical modelling. *Geomorphology*, *228*, 244–262.
- Hu, Z., Borsje, B. W., van Belzen, J., Willemsen, P. W., Wang, H., Peng, Y., Yuan, L., De Dominicis, M., Wolf, J., Temmerman, S., et al. (2021). Mechanistic modeling of marsh seedling establishment provides a positive outlook for coastal wetland restoration under global climate change. *Geophysical research letters*, *48*(22), e2021GL095596.
- Hu, Z., Van Belzen, J., Van Der Wal, D., Balke, T., Wang, Z. B., Stive, M., & Bouma, T. J. (2015). Windows of opportunity for salt marsh vegetation establishment on bare tidal flats: The importance of temporal and spatial variability in hydrodynamic forcing. *Journal of Geophysical Research: Biogeosciences*, *120*(7), 1450–1469.
- Hume, T. M. (1991). Empirical stability relationships for estuarine waterways and equations for stable channel design. *Journal of Coastal Research*, 1097–1111.
- Jarrett, J. T. (1976). *Tidal prism-inlet area relationships* (Vol. 3). US Army Engineer Waterways Experiment Station.
- Kalra, T. S., Ganju, N. K., Aretxabaleta, A. L., Carr, J. A., Defne, Z., & Moriarty, J. M. (2021). Modeling marsh dynamics using a 3-d coupled wave-flow-sediment model. *Frontiers in Marine Science*, *8*, 740921.
- Kernkamp, H. W., Van Dam, A., Stelling, G. S., & de Goede, E. D. (2011). Efficient scheme for the shallow water equations on unstructured grids with application to the continental shelf. *Ocean Dynamics*, *61*, 1175–1188.
- Kiesel, J., MacPherson, L. R., Schuerch, M., & Vafeidis, A. T. (2022). Can managed realignment buffer extreme surges? the relationship between marsh width, vegetation cover and surge attenuation. *Estuaries and Coasts*, *45*(2), 345–362.
- Kirwan, M. L., & Megonigal, J. P. (2013). Tidal wetland stability in the face of human impacts and sea-level rise. *Nature*, *504*(7478), 53–60.
- Kirwan, M. L., Temmerman, S., Skeehan, E. E., Guntenspergen, G. R., & Fagherazzi, S. (2016). Overestimation of marsh vulnerability to sea level rise. *Nature Climate Change*, *6*(3), 253–260.
- Ladd, C. J. T., Duggan-Edwards, M. F., Pagès, J. F., & Skov, M. W. (2021). Saltmarsh resilience to periodic shifts in tidal channels. *Frontiers in Marine Science*, *8*, 757715.
- Lawrence, P. J., Smith, G. R., Sullivan, M. J., & Mossman, H. L. (2018). Restored saltmarshes lack the topographic diversity found in natural habitat. *Ecological engineering*, *115*, 58–66.
- Lesser, G. R., Roelvink, J. v., van Kester, J. T. M., & Stelling, G. (2004). Development and validation of a three-dimensional morphological model. *Coastal engineering*, *51*(8-9), 883–915.
- Leuven, J. R. F. W., Verhoeve, S. L., Van Dijk, W. M., Selaković, S., & Kleinans, M. G. (2018). Empirical assessment tool for bathymetry, flow velocity and salinity in estuaries based on tidal amplitude and remotely-sensed imagery. *Remote Sensing*, *10*(12). <https://doi.org/10.3390/rs10121915>
- Liu, Z., Fagherazzi, S., & Cui, B. (2021). Success of coastal wetlands restoration is driven by sediment availability. *Communications Earth & Environment*, *2*(1), 44.
- Mariotti, G. (2020). Beyond marsh drowning: The many faces of marsh loss (and gain). *Advances in Water Resources*, *144*, 103710.
- Mariotti, G., & Canestrelli, A. (2017). Long-term morphodynamics of muddy backbarrier basins: Fill in or empty out? *Water Resources Research*, *53*(8), 7029–7054.

- Minderhoud, P., Erkens, G., Pham, V., Bui, V. T., Erban, L., Kooi, H., & Stouthamer, E. (2017). Impacts of 25 years of groundwater extraction on subsidence in the mekong delta, vietnam. *Environmental research letters*, *12*(6), 064006.
- Morris, J. T., Sundareshwar, P., Nietch, C. T., Kjerfve, B., & Cahoon, D. R. (2002). Responses of coastal wetlands to rising sea level. *Ecology*, *83*(10), 2869–2877.
- Morris, R. K. (2012). Managed realignment: A sediment management perspective. *Ocean & coastal management*, *65*, 59–66.
- Nicholls, R. J., & Cazenave, A. (2010). Sea-level rise and its impact on coastal zones. *science*, *328*(5985), 1517–1520.
- Norkko, A., Thrush, S. F., Hewitt, J. E., Cummings, V. J., Norkko, J., Ellis, J. I., Funnell, G. A., Schultz, D., & MacDonald, I. (2002). Smothering of estuarine sandflats by terrigenous clay: The role of wind-wave disturbance and bioturbation in site-dependent macrofaunal recovery. *Marine Ecology Progress Series*, *234*, 23–42.
- O'Brien, M. P. (1931). Estuary tidal prisms related to entrance areas. *Civil Engineering*.
- Oorschot, M. v., Kleinhans, M., Geerling, G., & Middelkoop, H. (2016). Distinct patterns of interaction between vegetation and morphodynamics. *Earth Surface Processes and Landforms*, *41*(6), 791–808.
- Partheniades, E. (1965). Erosion and deposition of cohesive soils. *Journal of the Hydraulics Division*, *91*(1), 105–139. <https://doi.org/10.1061/JYCEAJ.0001165>
- Pethick, J. (2002). Estuarine and tidal wetland restoration in the united kingdom: Policy versus practice. *Restoration ecology*, *10*(3), 431–437.
- Pontee, N., & Serato, B. (2019). Nearfield erosion at the steart marshes (uk) managed realignment scheme following opening. *Ocean & Coastal Management*, *172*, 64–81.
- Pontee, N. I. (2015). Impact of managed realignment design on estuarine water levels. *Proceedings of the Institution of Civil Engineers - Maritime Engineering*, *168*(2), 48–61. <https://doi.org/10.1680/jmaen.13.00016>
- Poppema, D. W., Willemsen, P. W., de Vries, M. B., Zhu, Z., Borsje, B. W., & Hulscher, S. J. (2019). Experiment-supported modelling of salt marsh establishment. *Ocean & coastal management*, *168*, 238–250.
- Rijkswaterstaat. (2023a). *Data register rijkswaterstaat*. Retrieved February 20, 2023, from <https://maps.rijkswaterstaat.nl/dataregister/srv/dut/catalog.search#/home>
- Rijkswaterstaat. (2023b). *Water info rijkswaterstaat*. Retrieved February 28, 2023, from <https://waterinfo.rws.nl/#!/nav/expert/>
- Roelvink, D. J., & Walstra, D.-J. (2005). Keeping it simple by using complex models. *Advances in Hydroscience and Engineering*, *6*.
- Roelvink, J. (2006). Coastal morphodynamic evolution techniques. *Coastal engineering*, *53*(2-3), 277–287.
- Schroevers, M., Huisman, B., Van Der Wal, M., & Terwindt, J. (2011). Measuring ship induced waves and currents on a tidal flat in the western scheldt estuary. *2011 IEEE/OES 10th Current, Waves and Turbulence Measurements (CWTM)*, 123–129.
- Schuerch, M., Spencer, T., Temmerman, S., Kirwan, M. L., Wolff, C., Lincke, D., McOwen, C. J., Pickering, M. D., Reef, R., Vafeidis, A. T., et al. (2018). Future response of global coastal wetlands to sea-level rise. *Nature*, *561*(7722), 231–234.
- Siemes, R. W., Duong, T. M., Willemsen, P. W., Borsje, B. W., & Hulscher, S. J. (in prep.). Modelling the eco-morphological response of a highly engineered estuary to altering channel depth and restoring wetlands.
- Soulsby, R. (1997). Dynamics of marine sands.

- Stive, M., Ji, L., Brouwer, R. L., van de Kreeke, C., & Ranasinghe, R. (2011). Empirical relationship between inlet cross-sectional area and tidal prism: A re-evaluation. *Coastal Engineering Proceedings*, (32), 86–86.
- Syvitski, J. P., Kettner, A. J., Overeem, I., Hutton, E. W., Hannon, M. T., Brakenridge, G. R., Day, J., Vörösmarty, C., Saito, Y., Giosan, L., et al. (2009). Sinking deltas due to human activities. *Nature Geoscience*, 2(10), 681–686.
- Temmerman, S., Bouma, T. J., Govers, G., Wang, Z., De Vries, M., & Herman, P. (2005). Impact of vegetation on flow routing and sedimentation patterns: Three-dimensional modeling for a tidal marsh. *Journal of Geophysical Research: Earth Surface*, 110(F4).
- Temmerman, S., Govers, G., Wartel, S., & Meire, P. (2004). Modelling estuarine variations in tidal marsh sedimentation: Response to changing sea level and suspended sediment concentrations. *Marine Geology*, 212(1-4), 1–19.
- Temmerman, S., & Kirwan, M. L. (2015). Building land with a rising sea. *science*, 349(6248), 588–589.
- Temmerman, S., Meire, P., Bouma, T. J., Herman, P. M., Ysebaert, T., & De Vriend, H. J. (2013). Ecosystem-based coastal defence in the face of global change. *Nature*, 504(7478), 79–83.
- Tessler, Z., Vörösmarty, C. J., Grossberg, M., Gladkova, I., Aizenman, H., Syvitski, J. P., & Foufoula-Georgiou, E. (2015). Profiling risk and sustainability in coastal deltas of the world. *Science*, 349(6248), 638–643.
- TNO. (2019). *Dino database, geotop version 1 release 4*. Retrieved November 20, 2022, from <https://www.dinoloket.nl/ondergrondmodellen>
- Townend, I. H. (2005). An examination of empirical stability relationships for uk estuaries. *Journal of Coastal Research*, 21(5), 1042–1053. Retrieved February 25, 2023, from <http://www.jstor.org/stable/4299504>
- Townend, I. H. (2008). Breach design for managed realignment sites. *Proceedings of the Institution of Civil Engineers - Maritime Engineering*, 161(1), 9–21. <https://doi.org/10.1680/maen.2008.161.1.9>
- Townend, I., & Pethick, J. (2002). Estuarine flooding and managed retreat. *Philosophical transactions. Series A, Mathematical, physical, and engineering sciences*, 360, 1477–95. <https://doi.org/10.1098/rsta.2002.1011>
- Townend, I., Scott, C., & Dixon, M. (2010). Managed realignment: A coastal flood management strategy. *Flood Risk Science and Management*, 60–86.
- van de Lageweg, W., de Paiva, J. S., van der Werf, J., de Vet, L., de Louw, P., Bouma, T., Walles, B., Ysebaert, T., & van Berchum, A. (2019). *Perkpolder tidal restoration*. Centre of Expertise Delta Technology.
- van der Wal, D., Wielemaker-van den Dool, A., & Herman, P. M. (2008). Spatial patterns, rates and mechanisms of saltmarsh cycles (westerschelde, the netherlands). *Estuarine, Coastal and Shelf Science*, 76(2), 357–368. <https://doi.org/https://doi.org/10.1016/j.ecss.2007.07.017>
- van der Vegt, H., & van der Wegen, M. (2021). *Invloed van erosieresistente lagen op morfologische verandering in de westerschelde*. Deltares.
- van der Wegen, M., Jaffe, B., Foxgrover, A., & Roelvink, D. (2017). Mudflat morphodynamics and the impact of sea level rise in south san francisco bay. *Estuaries and Coasts*, 40(1), 37–49.
- van Dongeren, A. (2018). *Implementation and verification of 2d coastal morphodynamic module in delft3d fm*. Retrieved September 20, 2022, from <https://www.slideshare.net/Delft-Software-Days/dsdint-2018-implementation-and-verification-of-2d-coastal-morphodynamic-module-in-delft3d-fm-van-dongeren>

- van Kessel, T., Vanlede, J., & de Kok, J. (2011). Development of a mud transport model for the scheldt estuary [Proceedings of the 9th International Conference on Nearshore and Estuarine Cohesive Sediment Transport Processes]. *Continental Shelf Research*, 31(10, Supplement), S165–S181. <https://doi.org/https://doi.org/10.1016/j.csr.2010.12.006>
- van Kessel, T., Vanlede, J., & de Kok, J. (2012). Bed module for sand-mud mixtures.
- van Ledden, M. (2003). *Sand-mud segregation in estuaries and tidal basins*. Delft University of Technology.
- van Rijn, L. C. (2007a). Unified view of sediment transport by currents and waves. i: Initiation of motion, bed roughness, and bed-load transport. *Journal of Hydraulic Engineering*, 133(6), 649–667. [https://doi.org/10.1061/\(ASCE\)0733-9429\(2007\)133:6\(649\)](https://doi.org/10.1061/(ASCE)0733-9429(2007)133:6(649))
- van Rijn, L. C. (2007b). Unified view of sediment transport by currents and waves. ii: Suspended transport. *Journal of Hydraulic Engineering*, 133(6), 668–689.
- van Belzen, J., Rienstra, G., & Bouma, T. (2021). *Dubbele dijken als robuuste waterkerende landschappen voor een welvarende zuidwestelijke delta*. NIOZ Koninklijk Nederlands Instituut voor Onderzoek der Zee.
- van Rijn, L. C., & Barth, R. (2019). Settling and consolidation of soft mud–sand layers. *Journal of Waterway, Port, Coastal, and Ocean Engineering*, 145(1), 04018028.
- Verbeek, H., van der Male, K., & Jansen, M. (2000). *Het scalwest-model(in dutch)* (tech. rep.). Rijksinstituut voor Kust en Zee/RIKZ.
- Vörösmarty, C., Syvitski, J., Day, J., de Sherbinin, A., Giosan, L., & Paola, C. (2009). Battling to save the world’s river deltas. *Bulletin of the Atomic Scientists*, 65(2), 31–43. <https://doi.org/10.2968/065002005>
- Vuik, V., Borsje, B. W., Willemsen, P. W., & Jonkman, S. N. (2019). Salt marshes for flood risk reduction: Quantifying long-term effectiveness and life-cycle costs. *Ocean & coastal management*, 171, 96–110.
- Wamsley, T. V., Cialone, M. A., Smith, J. M., Atkinson, J. H., & Rosati, J. D. (2010). The potential of wetlands in reducing storm surge. *Ocean Engineering*, 37(1), 59–68.
- Weisscher, S. A., Baar, A. W., van Belzen, J., Bouma, T. J., & Kleinhans, M. G. (2022). Transitional polders along estuaries: Driving land-level rise and reducing flood propagation. *Nature-Based Solutions*, 2, 100022. <https://doi.org/https://doi.org/10.1016/j.nbsj.2022.100022>
- Whitehouse, R., Soulsby, R., Roberts, W., & Mitchener, H. (2000). Dynamics of estuarine muds.
- Willemsen, P. W. J. M., Borsje, B. W., Hulscher, S. J. M. H., Van der Wal, D., Zhu, Z., Oteman, B., Evans, B., Möller, I., & Bouma, T. J. (2018). Quantifying bed level change at the transition of tidal flat and salt marsh: Can we understand the lateral location of the marsh edge? *Journal of Geophysical Research: Earth Surface*, 123(10), 2509–2524. <https://doi.org/https://doi.org/10.1029/2018JF004742>
- Williams, J. J., & Esteves, L. (2017). Guidance on setup, calibration, and validation of hydrodynamic, wave, and sediment models for shelf seas and estuaries. *Advances in civil engineering*, 2017.
- Winterwerp, J. C., Zhou, Z., Battista, G., Van Kessel, T., Jagers, H., Van Maren, D. S., & Van Der Wegen, M. (2018). Efficient consolidation model for morphodynamic simulations in low-spm environments. *Journal of Hydraulic Engineering*, 144(8), 04018055.
- Xu, Y., Kalra, T. S., Ganju, N. K., & Fagherazzi, S. (2022). Modeling the dynamics of salt marsh development in coastal land reclamation. *Geophysical Research Letters*, 49(6), e2021GL095559.
- Zhu, Z., Vuik, V., Visser, P. J., Soens, T., van Wesenbeeck, B., van de Koppel, J., Jonkman, S. N., Temmerman, S., & Bouma, T. J. (2020). Historic storms and the hidden value of coastal wetlands for nature-based flood defence. *Nature Sustainability*, 3(10), 853–862.

Appendices

A Model definition and input

A.1 Hydromorphological model description

The Delft3D Flexible Mesh (Delft3D-FM) process-based, numerical model was used in the current study to simulate hydrodynamics, sediment dynamics and morphological processes. This model and its predecessor Delft3D are widely used in coastal, estuarine and riverine systems (Kernkamp et al., 2011; Lesser et al., 2004; Oorschot et al., 2016)

The flow module D-Flow FM solves the unsteady shallow-water equations on an unstructured finite volume grid two dimensionally (depth-averaged, 2DH). Literature shows that a 2DH approach leads to similar results in terms of hydrodynamics and deposition rates as three-dimensional (3D) models (Horstman et al., 2015) in intertidal areas. In this sense we exclude the process of flow stratification due to salinity gradients in the intertidal zone, which lies outside of our interest and in return greatly reduce computation time. On the other hand, the use of an 1D model to describe hydromorphological evolution of an entire a wetland would not properly describe the spatial variation in the along estuary direction.

A.2 Sand-mud sediment transport

Estuaries such as the Western Scheldt typically consists of a range of sediments that have different grain sizes. Sediment particles can be split according to their grain size between cohesive and non-cohesive sediments. Larger sand particles ($> 63\mu m$) are single particles that are commonly described as spheres and are non-cohesive. However, finer mud particles ($< 63\mu m$) tend to flocculate and resemble thin plates, making them cohesive. Herein, the cohesive sediment is defined as the mixture of clay ($< 2\mu m$) and silt ($2-63\mu m$), wherein the clay fraction is cohesive. The flocculation behaviour of finer mud particles alters their behaviour as the plates become heavier and are thus less easily eroded. Therefore, a larger bed shear stress is needed to set these particles in suspension than one would infer from their grain size. Once eroded the smaller particles have a smaller settling velocity, remaining in suspension longer.

Critical mud content

The module distinguishes two erosional modes. Above a critical mud content ($p_{m,cr}$), cohesive particles cover sand particles so they are not in direct contact and sediment transport is completely governed by the erosional behaviour of the mud fraction. Below the critical mud fraction, the bed is defined as non-cohesive and a traditional sand transport equation is used. Cohesive properties become dominant when the clay fraction is larger than about 5-10%, which result in a critical mud (clay-silt) content of $p_{m,cr} = 0.2-0.4$ (van Ledden, 2003).

$$\tau_{cr} = \begin{cases} \tau_{cr,s} & p_{m,cr} < p_m \\ \tau_{cr,m} & p_{m,cr} \geq p_m \end{cases} \quad (\text{A.1})$$

Where τ_{cr} (N/m^2) is the critical shear stress for erosion and the subscript s and m represent the sand and mud sediment fraction respectively. Sand transport was calculated with van Rijn (2007a), which calculates the bed and suspended load and applicable to tidal environments. In the non-cohesive regime mud particles are washed out together with the sand particles. However, the presence of mud leads to a change in critical shear stress for the erosion of non-cohesive sediments (van Ledden, 2003). This increase in critical shear stress is determined by the fraction of mud (p_m) in the bed layer and a user defined parameter (default: $\beta_m = 3$). The critical bed shear stress of sand ($\tau_{s,cr}$) used in the erosion formula is then replaced by (after van Rijn, 2007a):

$$\tau_{cr,e} = \tau_{cr,s} (1 + p_m)^{\beta_m} \quad (\text{A.2})$$

Where $\tau_{cr,e}$ (N/m²) is the new critical shear stress for erosion of sand.

Layered bed stratigraphy

The stratigraphic bed module by van Kessel et al. (2011, 2012) tracks the spatial and temporal bed composition of layers of a user-defined thickness (Figure A.1). Erosion and deposition only occurs in the top layer (transport layer). Herein, the last deposited sediment is stored or sediment is repleted from deeper layers of previously deposited sediment.

, wherein the last deposited sediment is stored or eroded sediment is repleted from deeper layers of previously deposited sediment. The underlayers act a buffer for the transport layer. Sediment is supplied to the transport layer in case of erosion and stored in case of deposition. A user-defined number of layers need to be assigned. The sediment that is not able to be stored in the underlayers is stored in the base layer. Its thickness is not user-defined enabling storing all excess deposition. The transport and underlayers can be either:

- Lagrangian: Having a constant thickness and moving through the vertical frame with deposition and erosion. A constant thickness prevents strong bed armouring and the thickness affects the timescale of the system (van Kessel et al., 2012);
- Eulerian: Having a vertically fixed location and a variable thickness. The advantage of Eulerian layers is that artificial mixing by vertically moving layers is prevented.

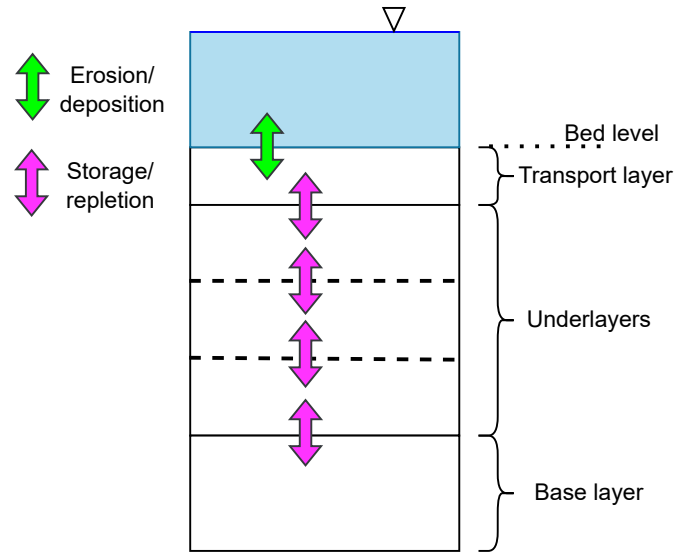


Figure A.1: Layered bed stratigraphy. Erosion and deposition only occurs between the transport layer and the water column.

A.3 Grid resolution

The total domain of the depth averaged-flow module is 14km in the alongshore direction and 3.7km in the cross-shore direction. The length in the alongshore direction is chosen such that the boundaries do not influence each other. The SSC is not able to travel the alongshore distance in half a tidal cycle (ebb to flood or vice versa). The cell size is 10x10m in the tidal basin and the near inlet area (Figure 2.3 bottom right). Grid coarsening is performed using triangular cells to greatly reduce computational effort. At a cross-shore distance of 2600m (Figure 2.3) and

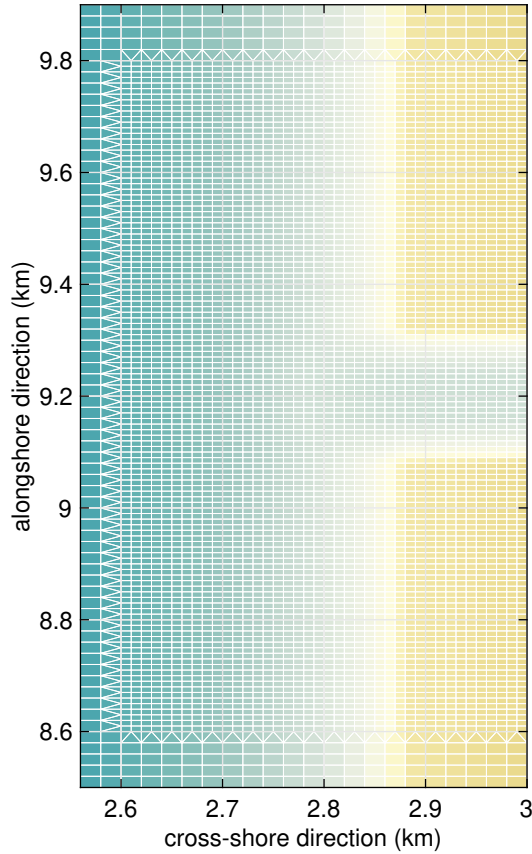


Figure A.2: Transition from 10x10m resolution to 20x20m via triangular cells outside of the managed realignment site.

between an alongshore distance of 8600m and 9600m (corresponding to the width of the tidal basin plus an arbitrary margin) the cell size is increased by a factor two (to 20x20m) by placing triangular cells (Figure A.2). From 2600m (and between 8600 and 9800m) to the edge of the estuarine channel the cell size in the cross-shore direction is gradually increased to 40m and remains 40m for the remainder of the estuarine channel. In the alongshore direction, the cell length outside of the width of the tidal basin (<8600 & >9800) is gradually increased to 60m. This way the grid is directed in the dominant flow direction and the grid resolution remains high in the areas of interest, while limiting computational power. The grid resolution is able to capture the largest channel forming (Best et al., 2018) in the tidal basin as present in salt marshes along the Western Scheldt estuary, while neglecting the smallest spatial scales.

A.4 Model parameters

Hydrodynamic model parameters

A uniform Manning bed roughness of $0.023\text{sm}^{-1/3}$ was used, which is slightly higher than the value for open waters (Wamsley et al., 2010), because of the interest in the intertidal area. Manning values are comparable with values used in previous studies on salt marshes in general and salt marshes in the Western Scheldt (Best et al., 2018; Willemsen et al., 2018). It should be noted that some studies use far higher values for manning in the presence of vegetation (Kiesel et al., 2022; Wamsley et al., 2010), as the increased roughness due to vegetation is not modelled explicitly (but incorporated in the Manning value). The horizontal eddy viscosity and eddy diffusivity are kept at the default value (Deltares, 2022a), recently changed in recent versions

of DFM (was $10m^2s^{-1}$)

DtMax/DtUser

D-Flow FM works with an automatic time step estimation that determines the maximum allowable cell timestep. This is partly based on the Courant-Friedrich-Lewy (CFL) number, where the flow is not allowed to travel more than the distance of a single cell in a single timestep. The unstructured grid has varying shapes and sizes, so the formulation is adapted. The adapted method checks the cell volume of the previous timestep against the sum of the total out flowing horizontal fluxes Deltares (2022a). In addition, the minimum timestep over all horizontal cells is taken and multiplied by the user defined CFL number (0.7).

Although the automatic timestep estimation is based on the CFL stability criteria, it can still cause unexpected oscillations. One way of solving this is lowering the maximum timestep DtMax of the model. Instabilities are mostly caused by large timesteps and the automatic time step criteria can lead to very high timestep estimations. Internal documents from Deltares have shown that D-morphology functions best for high MorFac and a low maximum timestep (van Dongeren, 2018). Therefore, the maximum timestep is set at 15s, relatively low compared to other modelling studies (Siemes et al., in prep. Willemsen et al., 2018).

Erosion of dry cells (ThetSD)

A problem that affect traditional numerical morphological models is that of bank erosion. This problem occurs where ‘wet’ or computationally active cells can erode, but ‘dry’ cells do not experience any change in sediment mass or bed elevation and can only be brought into the active domain of the water level rises sufficiently to cause inundation. The dry cell is unable to erode, even when considerable erosion occurs in a wet cell next to it. Therefore, dry breach and bank erosion was implemented to drive lateral bed lowering. A user-defined factor ThetSD = 0.5 (Braat et al., 2017) determines the fraction of the erosion flux that is assigned to adjacent dry cells.

Thatcher-Harleman lag time

The tides cause a change in flow direction, where flood transports water onto the wetland and during ebb the flow is in the direction of the estuary. During ebb flow a negative sediment transport out of the system occurs, which has a certain suspended sediment concentration. During flow the sediment concentration is given by the Dirichlet boundary condition at a constant rate. The discrepancy between these concentration can be problematic for numerical stability and realistic values in the system. To counter act this, a Thatcher-Harleman boundary conditions can be applied. This boundary conditions proposed that the sediment concentration at the switch between in and outflow is the same and that the proposed Dirichlet suspended sediment concentration is reached after a certain lag time. The lag time is set at 240 minutes (Best et al., 2018).

Transverse bed slope/AlfaBn The transverse bed slope determines magnitude of the sediment transport that is directed towards the downslope direction (Deltares, 2022b). As the transverse bed slope is based on the downward slope it only affects the bedload part of non-cohesive sediment. The transverse bed slope is a subject of many studies, with the most compelling by Baar et al. (2019). In this study the transverse transport is governed by the formulation of Ikeda (Deltares, 2022b), tuned by a user defined parameter AlfaBn. There are three main issues with the use of this parameter based on Baar et al. (2019):

1. The flow seems to prefer flowing through as few grid cells as possible. When grid cells are small more discharge flows through a smaller area and sharp channel incision occurs. This effect starts after approximately 10 years of morphological development.

2. The model has to overcome extreme incision by increasing the slope effect to model a dynamic system. Else, channels are not able to migrate and incise to severely. Only when grid size dependant incision is balanced by downslope sediment transport, the channel can migrate sideways.
3. The maximum value for which realistic sediment transport rates and direction are produced for of $\text{AlfaBn} = 5$. However, values >30 can be needed to overcome channel incision.

A value of $\text{AlfaBn} = 5$ is chosen for the current model, as a realistic sediment transport rate is deemed more important. However, its influence remains unknown and lies beyond the scope of this study.

A.5 Neumann boundary conditions

In order to produce the alongshore flow velocities as a result of tidal motion the method by Roelvink and Walstra (2005) is used to derive the boundary conditions. The method defines water levels along the offshore boundary and water level gradients along the cross-shore boundary for every tidal constituent. The water level for a tidal constituent in time is given by:

$$\zeta_j = \hat{\zeta}_j \cos(\omega_j t - \phi_j) \quad (\text{A.3})$$

where: $\hat{\zeta}_j$ = amplitude (m); T_j = Period (s); $\omega_j = \frac{2\pi}{T_j}$ angular frequency (rad/h); ϕ_j = phase difference (rad); The phase difference is given by:

$$\phi_j = k_j x = \frac{2\pi}{L_j} x \quad (\text{A.4})$$

Herein, x = position along the boundary (m); $k_j = \frac{2\pi}{L_j}$ wave number (rad/m); $L_j = \frac{2\pi}{\omega_j} c_j$ is the tidal wave length (m). The velocity of the tidal wave for shallow water is independent of the frequency and given by:

$$c_j = \sqrt{gH} \quad (\text{A.5})$$

With H a characteristic water depth and the earth gravity $g = 9.81 \text{ m/s}^2$. The water level along a boundary for a specific tidal constituent can now be calculated in space and time by the use of Equation A.3. The resulting water level is the sum of the water levels of N tidal constituents:

$$\zeta = \sum_{j=1}^N \zeta_j \quad (\text{A.6})$$

For the forcing of the cross-shore boundaries a gradient (Neumann) type of boundary condition is used. The gradient is related to water level of a tidal constituent by the relation:

$$\frac{\partial \zeta}{\partial x} = k_j \hat{\zeta}_j \sin(\omega_j t - k_j x) = k_j \hat{\zeta}_j \cos\left(\omega_j t - \left(\phi_j + \frac{\pi}{2}\right)\right) \quad (\text{A.7})$$

The resulting water level gradient is again the sum of the water level gradient of every tidal constituent. These types of boundary conditions can be applied for small coastal models to some degree. However, care should be taken in long morphodynamic simulations as the phase lag and water level gradient between the cross-shore boundaries are based on the long wave tidal characteristics, which is directly related to the maximum depth (or characteristic water depth H) at the alongshore boundary. Altering the morphology thus alters the phase lag and water

level gradients along the boundaries. However, the hydrodynamic boundary conditions are not altered during a simulation and can become unrealistic in relation to the estuary morphology. This is partly solved by providing a non-erodible layer in the deeper parts of the model, limiting the maximum depth, further explained in section 2.3.3.

B Regime channel

The regime channel method is based on mass continuity between the surface area and the vertical velocity of the water level (the volume of water going into the basin) and the horizontal velocity of the water and the inlet area (how is the increase in water level transported onto the tidal basin). The mass continuity is given by:

$$sv = ua = uhW \quad (\text{B.1})$$

The width for a rectangular basin is than calculated by:

$$W_b(t) = \frac{s(t)v(t)}{u_{cr}(t)h(t)} \quad (\text{B.2})$$

Where the vertical velocity is given by the change in water level as:

$$v(t) = \frac{d}{dt}\eta(t) \quad (\text{B.3})$$

Herein, the critical velocity that is likely to cause erosion is found by setting $\tau_0 = \tau_{cr}$, the shear stress at erosion threshold. The critical shear is dependent on the local sediment. If no data on local sediments is available, one can estimate it from Whitehouse et al. (2000, p. 65) for fine silts and mud (cohesive sediments) and from Soulsby (1997, p.104) for marine sands (non-cohesive). From the critical shear stress the friction velocity and roughness length can be calculated.

$$u_* = \sqrt{\frac{\tau_{cr}}{\rho_w}} \quad (\text{B.4})$$

$$z_0 = \frac{k_s}{30} \left[1 - \exp\left(-\frac{uk_s}{27v}\right) \right] + \frac{v}{9u_*} \quad (\text{B.5})$$

And the depth-averaged velocity that gives rise to the critical shear stress (τ_{cr}) is given by:

$$u_{cr}(h) = \frac{u_*}{\kappa} \left[\ln\left(\frac{h}{z_0}\right) - 1 \right] \quad (\text{B.6})$$

A rectangular width can now be easily calculated for a specific hydraulic depth by filling Eq. B.2 for the calculated velocity. Townend (2008) has shown that a rectangular channels underestimates the width of the breach by a factor two and thus an adaptation of the method is suggested based on a discharge based regime relationship. The full method is explained further and in more detail in Townend (2008).

C Results

C.1 Model artifacts

All model scenarios show a huge amount of sediment at the western boundary. This is caused by and extra boundary point at a cross-shore coordinate of 9200m. The cross-shore amplitude

of the flow velocity decreases the further away a location is from the extra boundary points (Figure C.1). The differences in flow velocities induce a difference in sediment transport. The small differences in sediment transport grows into the huge amount of sedimentation along the western boundary. Although the formation of mid channel shoals is not uncommon in the Western Scheldt, the sedimentation is a clear model artifact. In spite of the created shoal, the boundaries are still able to produce the motion of the tidal wave over the full length of the simulation.

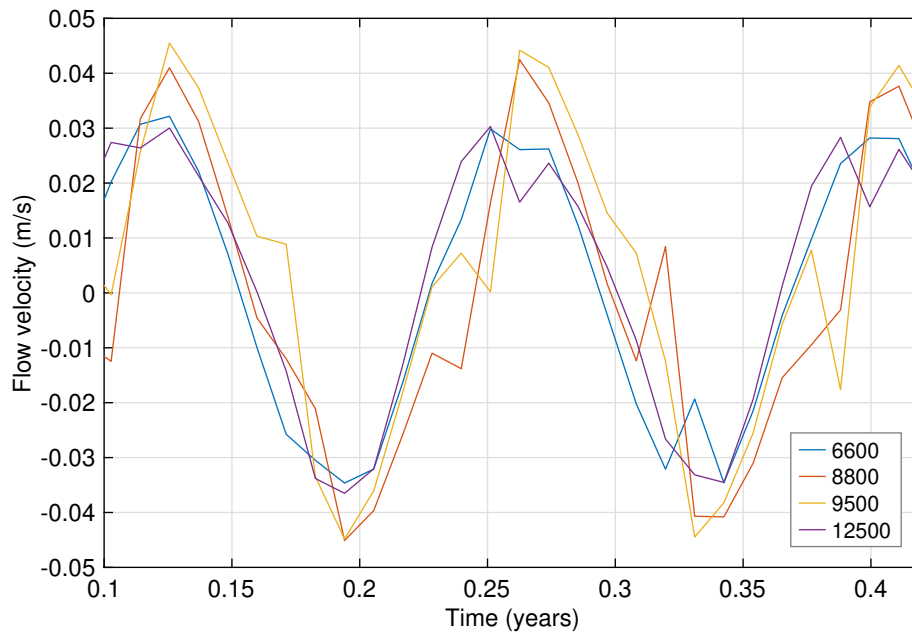


Figure C.1: Cross-shore velocity at different points along the Western Boundary. Extra boundary points is at a cross-shore coordinate of 9200m

C.2 Hydrodynamics

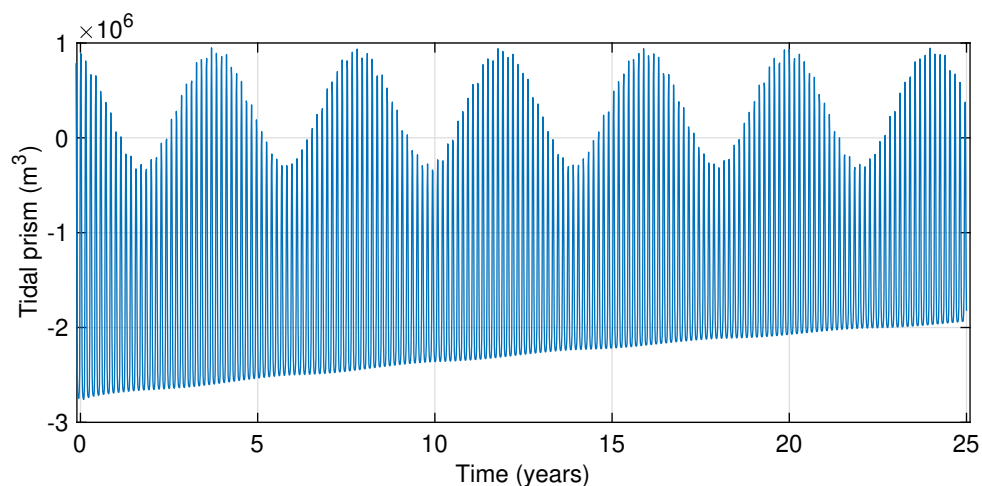


Figure C.2: Development of the tidal prism of the reference scenario over time. The tidal prism reduces over time as a results of the morphological development of the system. Tidal prism is based on cumulative discharge through the inlet. Therefore, the negative values represent the volume of water based the initial volume present in the managed realignment site.

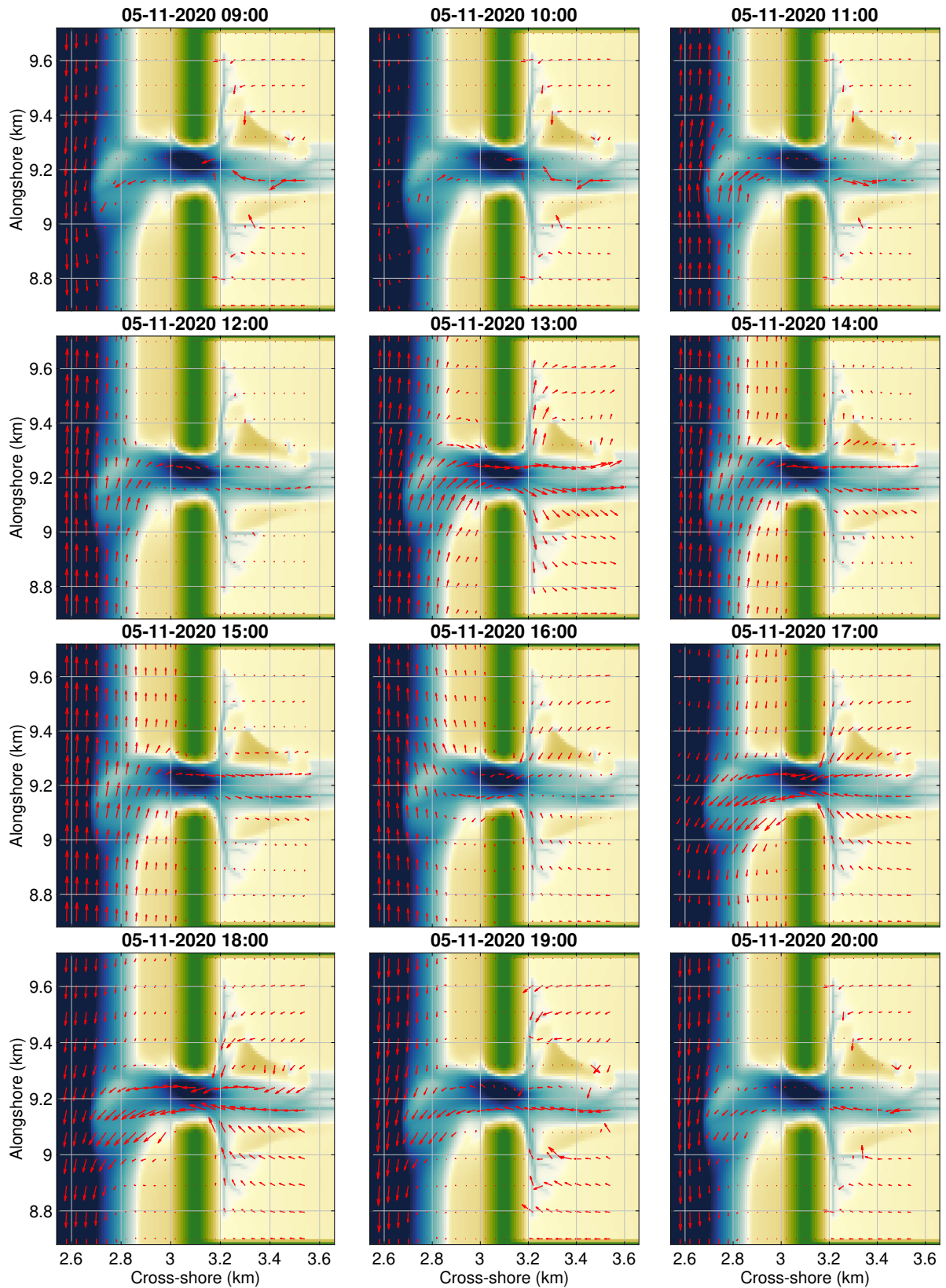


Figure C.3: Flow velocities over an entire tidal cycle after 1 year of morphological development between 15-Nov 09:00 and 15-Nov 18:00